PHYSICAL REVIEW B **94**, 125301 (2016)

Ab initio description of second-harmonic generation from crystal surfaces

Nicolas Tancogne-Dejean, Christine Giorgetti, and Valérie Véniard[*]
Laboratoire des Solides Irradiés, Ecole polytechnique, CNRS, CEA, Université Paris-Saclay, 91128 Palaiseau, France
and European Theoretical Spectroscopy Facility, 91128 Palaiseau, France

(Received 7 April 2016; revised manuscript received 22 July 2016; published 6 September 2016)

We propose an *ab initio* framework to derive the dielectric and the second-order susceptibility tensors for crystal surfaces. The single-surface response is extracted from a supercell scheme. We evaluate macroscopic quantities, taking into account the local fields. The first- and second-order susceptibilities are evaluated within time-dependent density functional theory, in the long-wavelength limit. We apply our formalism to the calculation of the second-harmonic generation for clean and hydrogenated silicon surfaces. The agreement with measured second-order susceptibility components is significantly better, illustrating the importance of local-field effects.

DOI: 10.1103/PhysRevB.94.125301

I. INTRODUCTION

Second-harmonic generation (SHG) is a process where two photons at a given energy are absorbed and one photon at twice this energy is emitted. It is particularly suited for surface studies due to its high sensitivity to the symmetries of the system. Indeed, within the dipole approximation, the SHG is zero for centrosymmetric materials and thus it can only originate from symmetry-breaking regions. This makes SHG an extremely versatile tool for studying surfaces [1,2], superlattices [3], and interfaces [4,5]. Nowadays, this technique is used to characterize systems such as nanomaterials [6–12]. Furthermore, SHG is also interesting for the development of optoelectronic devices [13–16].

From the theoretical point of view, the correct evaluation of the second-order susceptibility is cumbersome, as it has to include the many-body interactions between the electrons of the system: the variation of the screening fields on the microscopic scale, i.e., local-field effects (LFEs), as well as the electron-hole interaction, i.e., excitonic effects. However, recent progress has been achieved for bulk systems [17–23].

For surfaces, the theoretical description of optical properties suffers from even more difficulties, linked to the need to describe a semi-infinite system [24]. Since the surface keeps two-dimensional in-plane periodicity, the use of a plane-wave basis set in reciprocal space appears appropriate to study these systems. Most of the numerical implementations used in condensed matter rely on three-dimensional periodic boundary conditions and the standard way to model a surface is to use a slab of matter, embedded in a supercell with vacuum [24–28].

Concerning the optical linear properties, calculations in the independent-particle approximation (IPA), i.e., neglecting local field and excitonic effects, have been performed for the in-plane components, giving satisfactory results when compared to experimental results [25,29]. However, due to the abrupt change in the electronic density at the surface, the local fields (LFs) are expected to play a key role perpendicularly to the surface plane. Their impact has been discussed for years and analytic expressions for the surface response have been presented, but their numerical evaluation has often been restricted to simple cases [30–33]. Recently, we have proposed an *ab initio* framework, called "Selected-**G**," allowing the calculation of optical absorption spectra for surfaces, including local fields for in-plane and out-of-plane components in a supercell approach [24].

Additional difficulties appear for SHG when evaluated within a supercell: the slab is composed of two surfaces and the response of the two surfaces interferes in a destructive way. This is not the case for the linear case, since constructive interferences occur [34–36]. This has been solved within IPA, using the so-called cut function, in order to extract the response of only one-half of the slab [36–40].

Due to the difficulties in the calculation, LFEs on surface second-harmonic generation have often been neglected [34–41] or estimated using models fitted on experimental data [42,43]. Understanding, by means of *ab initio* methods, how local-field effects affect the second-harmonic generation at crystal surfaces is the aim of this paper. The existing theory, developed for bulk SHG [17], must be modified in order to include the cut function in the macroscopic formalism.

This paper is organized as follows. In Sec. II, we present the analytic derivation of the microscopic polarization up to second order in terms of the total electric field. It allows us to establish the expression of the electric displacement as an explicit function of the spatial coordinate perpendicular to the surface plane. From that expression, we define in Sec. III the surface macroscopic dielectric tensor in the optical limit and make the link with time-dependent density functional theory (TDDFT). Following the same procedure, the derivation for second-order macroscopic susceptibility is presented in Sec. IV. In the last part, we apply our formalism to calculate the surface second-harmonic generation of clean and hydrogenated silicon surfaces: the dihydride Si(001)1 × 1:2H, the monohydride Si(001)2 × 1:H, and the clean Si(001)2 × 1.

II. MICROSCOPIC POLARIZATION

We consider a dielectric material, perturbed by an external field $\mathbf{E}^{\mathrm{ext}}$. Following the paper of Del Sole and Fiorino [30], we express the polarization as the response to a perturbing field $\mathbf{E}^{P}$ defined as

$$\mathbf{E}^{P} = \mathbf{E}^{\mathrm{ext}} + \mathbf{E}^{i,T} = \mathbf{E} - \mathbf{E}^{i,L}, \tag{1}$$

---

[*] valerie.veniard@polytechnique.fr

where $\mathbf{E}$ is the total microscopic field, and $\mathbf{E}^{i,T}$ and $\mathbf{E}^{i,L}$ are, respectively, the transverse and the longitudinal components of the field induced by the external perturbation.

Using the electric displacement vector $\mathbf{D} = \mathbf{E} + 4\pi\mathbf{P}$ and taking into account the relation $D^{L}_{\mathbf{G}}(\mathbf{q}) = E^{\mathrm{ext,L}}_{\mathbf{G}}(\mathbf{q})$, one gets $E^{i,L}_{\mathbf{G}}(\mathbf{q}) = -4\pi P^{L}_{\mathbf{G}}(\mathbf{q})$, where $P_{\mathbf{G}}(\mathbf{q})$ stands for $P(\mathbf{q}+\mathbf{G})$, with $\mathbf{q}$ a vector in the first Brillouin zone (BZ) and $\mathbf{G}$ a vector of the reciprocal lattice. The total electric field $\mathbf{E} = \mathbf{E}^{p} + \mathbf{E}^{i,L}$ becomes

$$\mathbf{E}_{\mathbf{G}}(\mathbf{q};\omega) = \mathbf{E}^{p}_{\mathbf{G}}(\mathbf{q};\omega) - 4\pi \frac{\mathbf{q}+\mathbf{G}}{|\mathbf{q}+\mathbf{G}|} P^{L}_{\mathbf{G}}(\mathbf{q};\omega), \tag{2}$$

and its macroscopic average corresponds to the $\mathbf{G} = \mathbf{0}$ component [44],

$$\mathbf{E}_{\mathbf{0}}(\mathbf{q};\omega) = \mathbf{E}^{p}_{\mathbf{0}}(\mathbf{q};\omega) - 4\pi \frac{\mathbf{q}}{|\mathbf{q}|} P^{L}_{\mathbf{0}}(\mathbf{q};\omega). \tag{3}$$

The polarization will be first expanded to second order in terms of the perturbing electric field: $\mathbf{P} = \mathbf{P}^{(1)} + \mathbf{P}^{(2)}$. As it was shown in Ref. [30] that E^{P} is a macroscopic quantity, the polarizations are expressed as

$$\mathbf{P}^{(1)}_{\mathbf{G}}(\mathbf{q};\omega) = \overleftrightarrow{\tilde{\alpha}}^{(1)}_{\mathbf{G0}}(\mathbf{q},\mathbf{q};\omega)\mathbf{E}^{P}_{\mathbf{0}}(\mathbf{q};\omega) \tag{4}$$

and

$$\begin{aligned}\mathbf{P}^{(2)}_{\mathbf{G}}&(\mathbf{q};\omega)\\ &= \sum_{\mathbf{q}_1\mathbf{q}_2} \delta_{\mathbf{q},\mathbf{q}_1+\mathbf{q}_2} \int d\omega_1 d\omega_2 \delta(\omega-\omega_1-\omega_2)\\ &\quad\times \overleftrightarrow{\tilde{\alpha}}^{(2)}_{\mathbf{G00}}(\mathbf{q},\mathbf{q}_1,\mathbf{q}_2;\omega,\omega_1,\omega_2)\mathbf{E}^{P}_{\mathbf{0}}(\mathbf{q}_1;\omega_1)\mathbf{E}^{P}_{\mathbf{0}}(\mathbf{q}_2;\omega_2).\end{aligned} \tag{5}$$

The quantities $\overleftrightarrow{\tilde{\alpha}}^{(1)}$ and $\overleftrightarrow{\tilde{\alpha}}^{(2)}$ are, respectively, the linear and second-order quasipolarizability, defined in terms of current response functions, $\chi_{\mathbf{jj}}$ and $\chi_{\mathbf{jjj}}$ [17,30]. Inserting Eq. (3) in Eq. (4), we get, for $\mathbf{P}^{(1)}$,

$$\begin{aligned}\mathbf{P}^{(1)}_{\mathbf{G}}(\mathbf{q};\omega) &= \overleftrightarrow{\tilde{\alpha}}^{(1)}_{\mathbf{G0}}(\mathbf{q},\mathbf{q};\omega)\mathbf{E}_{\mathbf{0}}(\mathbf{q};\omega)\\ &\quad +4\pi\, \overleftrightarrow{\tilde{\alpha}}^{(1)}_{\mathbf{G0}}(\mathbf{q},\mathbf{q};\omega)\frac{\mathbf{q}}{|\mathbf{q}|}\,\frac{\mathbf{q}}{|\mathbf{q}|}\\ &\quad \times \big[\mathbf{P}^{(1)}_{\mathbf{0}}(\mathbf{q};\omega) + \mathbf{P}^{(2)}_{\mathbf{0}}(\mathbf{q};\omega)\big].\end{aligned} \tag{6}$$

This equation is solved in two steps, with the first one consisting of setting $\mathbf{G} = 0$ in the equation and then using the result to get $\mathbf{P}^{(1)}_{\mathbf{G}}(\mathbf{q};\omega)$ for any $\mathbf{G}$ vector. It gives, for $\mathbf{P}^{(1)}_{\mathbf{0}}(\mathbf{q};\omega)$,

$$\begin{aligned}\mathbf{P}^{(1)}_{\mathbf{0}}(\mathbf{q};\omega) &= \overleftrightarrow{\tilde{\alpha}}^{(1)}_{\mathbf{00}}(\mathbf{q},\mathbf{q};\omega)A(\mathbf{q};\omega)\mathbf{E}_{\mathbf{0}}(\mathbf{q};\omega)\\ &\quad +4\pi\, \overleftrightarrow{\tilde{\alpha}}^{(1)}_{\mathbf{00}}(\mathbf{q},\mathbf{q};\omega)A(\mathbf{q};\omega)\frac{\mathbf{q}}{|\mathbf{q}|}\,\frac{\mathbf{q}}{|\mathbf{q}|}\mathbf{P}^{(2)}_{\mathbf{0}}(\mathbf{q};\omega),\end{aligned} \tag{7}$$

with

$$\overleftrightarrow{A}(\mathbf{q};\omega) = 1 + 4\pi\, \frac{\mathbf{q}}{|\mathbf{q}|}\,\frac{\mathbf{q}}{|\mathbf{q}|}\,\frac{\overleftrightarrow{\tilde{\alpha}}^{(1)}_{\mathbf{00}}(\mathbf{q},\mathbf{q};\omega)}{1-4\pi\tilde{\alpha}^{(1),LL}_{\mathbf{00}}(\mathbf{q},\mathbf{q};\omega)}. \tag{8}$$

Inserting Eq. (7) into Eq. (6), we get

$$\begin{aligned}\mathbf{P}^{(1)}_{\mathbf{G}}(\mathbf{q};\omega) &= \overleftrightarrow{\tilde{\alpha}}^{(1)}_{\mathbf{G0}}(\mathbf{q},\mathbf{q};\omega)\,\overleftrightarrow{A}(\mathbf{q};\omega)\mathbf{E}_{\mathbf{0}}(\mathbf{q};\omega)\\ &\quad +4\pi\, \overleftrightarrow{\tilde{\alpha}}^{(1)}_{\mathbf{G0}}(\mathbf{q},\mathbf{q};\omega)\,\overleftrightarrow{A}(\mathbf{q};\omega)\frac{\mathbf{q}}{|\mathbf{q}|}\,\frac{\mathbf{q}}{|\mathbf{q}|}\mathbf{P}^{(2)}_{\mathbf{0}}(\mathbf{q};\omega).\end{aligned} \tag{9}$$

The second-order polarization $\mathbf{P}^{(2)}$ is obtained from Eq. (5), while keeping only the first-order term in P^{L}_{0} in Eq. (3),

$$\mathbf{E}^{P}_{\mathbf{0}}(\mathbf{q};\omega) = \overleftrightarrow{A}(\mathbf{q};\omega)\mathbf{E}_{\mathbf{0}}(\mathbf{q};\omega), \tag{10}$$

which gives

$$\begin{aligned}\mathbf{P}^{(2)}_{\mathbf{G}}(\mathbf{q};\omega) &= \sum_{\mathbf{q}_1\mathbf{q}_2} \delta_{\mathbf{q},\mathbf{q}_1+\mathbf{q}_2} \int d\omega_1 d\omega_2 \delta(\omega-\omega_1-\omega_2)\\ &\quad\times \overleftrightarrow{\tilde{\alpha}}^{(2)}_{\mathbf{G00}}(\mathbf{q},\mathbf{q}_1,\mathbf{q}_2;\omega,\omega_1,\omega_2)\,\overleftrightarrow{A}(\mathbf{q}_1;\omega_1)\\ &\quad\times \mathbf{E}_{\mathbf{0}}(\mathbf{q}_1;\omega_1)\,\overleftrightarrow{A}(\mathbf{q}_2;\omega_2)\mathbf{E}_{\mathbf{0}}(\mathbf{q}_2;\omega_2).\end{aligned} \tag{11}$$

Coming back to the expression of the electric displacement vector $\mathbf{D}$, it appears that it can be expressed as a sum of the first-order and second-order terms in the total electric field,

$$\mathbf{D}^{(1)}_{\mathbf{G}}(\mathbf{q};\omega) = E_{\mathbf{G}}(\mathbf{q};\omega) + 4\pi\, \overleftrightarrow{\tilde{\alpha}}^{(1)}_{\mathbf{G0}}(\mathbf{q},\mathbf{q};\omega)\,\overleftrightarrow{A}(\mathbf{q};\omega)\mathbf{E}_{\mathbf{0}}(\mathbf{q};\omega) \tag{12}$$

and

$$\begin{aligned}\mathbf{D}^{(2)}_{\mathbf{G}}(\mathbf{q};\omega) &= 4\pi \sum_{\mathbf{q}_1\mathbf{q}_2} \delta_{\mathbf{q},\mathbf{q}_1+\mathbf{q}_2} \int d\omega_1 d\omega_2 \delta(\omega-\omega_1-\omega_2)\\ &\quad + \left[4\pi\, \overleftrightarrow{\tilde{\alpha}}^{(1)}_{\mathbf{G0}}(\mathbf{q},\mathbf{q};\omega)\,\overleftrightarrow{A}(\mathbf{q};\omega)\frac{\mathbf{q}}{|\mathbf{q}|}\,\frac{\mathbf{q}}{|\mathbf{q}|}\,\overleftrightarrow{\tilde{\alpha}}^{(2)}_{\mathbf{000}}(\mathbf{q},\mathbf{q}_1,\mathbf{q}_2;\omega,\omega_1,\omega_2)\,\overleftrightarrow{\tilde{\alpha}}^{(2)}_{\mathbf{G00}}(\mathbf{q},\mathbf{q}_1,\mathbf{q}_2;\omega,\omega_1,\omega_2)\right]\\ &\quad \times \overleftrightarrow{A}(\mathbf{q}_1;\omega_1)\,\overleftrightarrow{A}(\mathbf{q}_2;\omega_2)\mathbf{E}_{\mathbf{0}}(\mathbf{q}_1;\omega_1)\mathbf{E}_{\mathbf{0}}(\mathbf{q}_2;\omega_2).\end{aligned} \tag{13}$$

These formulas, general and valid for any periodic system, are the starting points for macroscopic average.

We now consider the case of a supercell, containing N atomic layers, corresponding to a thickness L_z and a vacuum region of the same thickness, where z is the direction perpendicular to the surface. In order to average over a selected region of the slab, we express the electric displacement in a mixed space, where the in-plane periodicity is treated in reciprocal space and the out-of-plane direction is treated in real space.

The definitions of Fourier transforms can be found in Appendix A. Using Def. (A2), we obtain

$$\mathbf{D}_{\mathbf{G}_{||}}(\mathbf{q}_{||},z;\omega) = \frac{1}{2L_z}\sum_{q_z G_z} e^{i(q_z+G_z)z}\mathbf{D}_{\mathbf{G}}(\mathbf{q};\omega). \tag{14}$$

With the expression of the total electric field, $\mathbf{E_0}(\mathbf{q};\omega) = \int dz' e^{-iq_z z'} \mathbf{E_0}(\mathbf{q}_{||},z';\omega)$, the electric displacement vector in the mixed space reads

$$\begin{aligned}\mathbf{D}^{(1)}_{\mathbf{G}_{||}}(\mathbf{q}_{||},z;\omega) &= \mathbf{E}_{\mathbf{G}_{||}}(\mathbf{q}_{||},z;\omega) + \frac{4\pi}{2L_z}\sum_{q_z G_z} e^{i(q_z+G_z)z}\, \overset{\leftrightarrow}{\tilde{\alpha}}{}^{(1)}_{\mathbf{G0}}(\mathbf{q},\mathbf{q};\omega)\, \overset{\leftrightarrow}{A}(\mathbf{q};\omega)\mathbf{E_0}(\mathbf{q};\omega) \\ &= \int dz' \left[\mathbf{E}_{\mathbf{G}_{||}}(\mathbf{q}_{||},z';\omega)\delta(z-z') + \frac{4\pi}{2L_z}\sum_{q_z G_z} e^{i(q_z+G_z)z}\, \overset{\leftrightarrow}{\tilde{\alpha}}{}^{(1)}_{\mathbf{G0}}(\mathbf{q},\mathbf{q};\omega)_{\mathbf{G_z0}}\, \overset{\leftrightarrow}{A}(\mathbf{q};\omega)e^{-iq_z z'}\mathbf{E_0}(\mathbf{q}_{||},z';\omega)\right] \qquad (15)\end{aligned}$$

and

$$\begin{aligned}\mathbf{D}^{(2)}_{\mathbf{G}_{||}}(\mathbf{q}_{||},z;\omega) = \frac{(4\pi)}{2L_z}&\int dz' dz'' \sum_{\mathbf{q}_1\mathbf{q}_2} \delta_{\mathbf{q},\mathbf{q}_1+\mathbf{q}_2} \int d\omega_1 d\omega_2 \delta(\omega-\omega_1-\omega_2) \sum_{q_z,G_z} e^{i(q_z+G_z)z} \\ &\times\left[4\pi\, \overset{\leftrightarrow}{\tilde{\alpha}}{}^{(1)}_{\mathbf{G0}}(\mathbf{q},\mathbf{q};\omega)\, \overset{\leftrightarrow}{A}(\mathbf{q};\omega)\frac{\mathbf{q}}{|\mathbf{q}|}\frac{\mathbf{q}}{|\mathbf{q}|}\, \overset{\leftrightarrow}{\tilde{\alpha}}{}^{(2)}_{\mathbf{G00}}(\mathbf{q},\mathbf{q}_1,\mathbf{q}_2;\omega,\omega_1,\omega_2) + \overset{\leftrightarrow}{\tilde{\alpha}}{}^{(2)}_{\mathbf{G00}}(\mathbf{q},\mathbf{q}_1,\mathbf{q}_2;\omega,\omega_1,\omega_2)\right] \\ &\times e^{-iq_{1z}z'} e^{-iq_{2z}z''}\, \overset{\leftrightarrow}{A}(\mathbf{q}_1;\omega_1)\, \overset{\leftrightarrow}{A}(\mathbf{q}_2;\omega_2)\mathbf{E_0}(\mathbf{q_1}_{||},z';\omega_1)\mathbf{E_0}(\mathbf{q_2}_{||},z'';\omega_2). \qquad (16)\end{aligned}$$

III. MACROSCOPIC DIELECTRIC TENSOR OF CRYSTAL SURFACES

A. Surface average of ϵ

The in-plane averaged macroscopic dielectric tensor is defined by $\mathbf{D}^{(1)}_{\mathbf{0}}(\mathbf{q}_{||},z;\omega) = \int dz'\, \overset{\leftrightarrow}{\epsilon}_m(\mathbf{q}_{||},z,z';\omega)\mathbf{E_0}(\mathbf{q}_{||},z';\omega)$. With the expression of $\mathbf{D}^{(1)}$ given in Eq. (15), for $\mathbf{G}_{||} = 0$, one gets

$$\begin{aligned}\overset{\leftrightarrow}{\epsilon}_m(\mathbf{q}_{||},z,z';\omega) = \overset{\leftrightarrow}{\mathbb{1}}\,\delta(z-z') + \frac{4\pi}{2L_z}\sum_{q_z G_z} e^{i(q_z+G_z)z}\, \overset{\leftrightarrow}{\alpha}{}^{(1)}_{\mathbf{G_z0}} \\ \times(\mathbf{q},\mathbf{q};\omega)\, \overset{\leftrightarrow}{A}(\mathbf{q};\omega)e^{-iq_z z'}. \qquad (17)\end{aligned}$$

This quantity still contains the microscopic fluctuations along the z direction [33]. In the following, m will be used for in-plane macroscopic averaged quantities, while M will refer to the three-dimensional (3D) macroscopic average.

We define the surface macroscopic quantities as the macroscopic average over half of the cell. For the surface macroscopic dielectric tensor, we get

$$\overset{\leftrightarrow}{\epsilon}{}^{S}_{M}(\mathbf{q};\omega) = \frac{1}{L_z}\int_{-L_z}^{0} dz dz'\, \overset{\leftrightarrow}{\epsilon}_m(\mathbf{q}_{||},z,z';\omega)e^{-iq_z(z-z')}, \qquad (18)$$

which can be written as

$$\overset{\leftrightarrow}{\epsilon}{}^{S}_{M}(\mathbf{q};\omega) = \frac{1}{L_z}\int_{-L_z}^{L_z} dz dz' \mathcal{C}(z)\, \overset{\leftrightarrow}{\epsilon}_m(\mathbf{q}_{||},z,z';\omega)e^{-iq_z(z-z')}, \qquad (19)$$

where $\mathcal{C}(z)$ is a cut function equal to 1 on one half of the supercell and 0 on the other half, as previously introduced (see, for instance, Refs. [36,41,45]) and illustrated in Fig. 1. This shape for $\mathcal{C}(z)$ will be justified later in the paper.

This dielectric tensor, called here the surface dielectric tensor, fully accounts for the surface-induced modification of the bulk material: it contains the modification of the electronic structure at the microscopic level, including possible surface states, and at a macroscopic level, taking into account the (surface) local-field effects.

Combining Eqs. (17) and (19), we obtain an expression for the macroscopic surface dielectric tensor,

$$\begin{aligned}\overset{\leftrightarrow}{\epsilon}{}^{S}_{M}(\mathbf{q}) &= \overset{\leftrightarrow}{\mathbb{1}} + \frac{4\pi}{L_z}\sum_{G_z}\tilde{\mathcal{C}}(G_z)\, \overset{\leftrightarrow}{\tilde{\alpha}}{}^{(1)}_{\mathbf{G_z0}}(\mathbf{q},\mathbf{q})\, \overset{\leftrightarrow}{A}(\mathbf{q}) \\ &= \overset{\leftrightarrow}{\mathbb{1}} + 4\pi\, \overset{\leftrightarrow}{\tilde{\alpha}}{}^{(1)S}(\mathbf{q})\, \overset{\leftrightarrow}{A}(\mathbf{q}), \qquad (20)\end{aligned}$$

where $\overset{\leftrightarrow}{\tilde{\alpha}}{}^{(1)S}$ is defined by the last part of the equation.

Replacing $\overset{\leftrightarrow}{A}$ by its definition [see Eq. (8)], one directly gets

$$\begin{aligned}\overset{\leftrightarrow}{\epsilon}{}^{S}_{M}(\mathbf{q}) = \overset{\leftrightarrow}{\mathbb{1}} + 4\pi\, \overset{\leftrightarrow}{\tilde{\alpha}}{}^{(1)S}(\mathbf{q}) \\ \times\left[\overset{\leftrightarrow}{1} + 4\pi\frac{\mathbf{q}}{|\mathbf{q}|}\frac{\mathbf{q}}{|\mathbf{q}|}\frac{\overset{\leftrightarrow}{\tilde{\alpha}}{}^{(1)}_{\mathbf{00}}(\mathbf{q},\mathbf{q})}{1-4\pi\tilde{\alpha}^{(1)LL}_{\mathbf{00}}(\mathbf{q},\mathbf{q})}\right]. \qquad (21)\end{aligned}$$

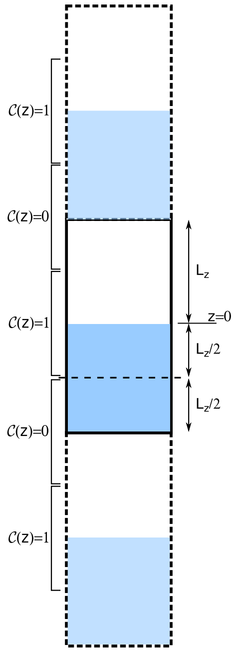

FIG. 1. Slab geometry and the $\mathcal{C}(z)$ function. The surface is located at $z = 0$, and $\mathcal{C}(z) = 1$ covers half of the matter (and half of the vacuum) to define one single surface.

This expression is very similar to the Del Sole and Fiorino expression (see Eq. (25) of Ref. [30]), except that here we have surface quantities. In Ref. [30], the authors also obtained expressions for macroscopic surface quantities, but in terms of inverse integral operators. It comes from the fact that they describe the surface by a semi-infinite medium, implying a continuous variable along the z-reciprocal direction. In the present paper, we chose to describe the surface using a supercell approach, which allows us to solve matrix equations.

We also remark that not all ingredients in the definition of $\overset{\leftrightarrow}{\epsilon}{}^{S}_{M}(\mathbf{q})$ are modified by the presence of the surface.

B. Optical limit for the surface macroscopic dielectric function

In the following, we focus our discussion on the optical limit, which corresponds to the case of a perturbation with a vanishing momentum. The key quantity is the longitudinal-longitudinal (LL) part of the macroscopic dielectric function $\epsilon_M^{S,LL}$, which can be evaluated in the framework of TDDFT.

From Eq. (21), the LL part of the surface macroscopic dielectric tensor reads

$$\epsilon_M^{S,LL}(\hat{\mathbf{q}};\omega) = 1 + \lim_{\mathbf{q}\to\mathbf{0}} \frac{4\pi\tilde{\alpha}^{(1)S,LL}(\mathbf{q},\mathbf{q};\omega)}{1 - 4\pi\tilde{\alpha}^{(1)LL}_{\mathbf{00}}(\mathbf{q},\mathbf{q},\omega)}, \tag{22}$$

where $\hat{\mathbf{q}}$ is the unit vector along $\mathbf{q}$. At this point, in order to calculate $\tilde{\alpha}^{(1)S,LL}$, we come back to the definition of the quasipolarizability $\overset{\leftrightarrow}{\tilde{\alpha}}{}^{(1)}$ in terms of response functions [44]

$$\overset{\leftrightarrow}{\tilde{\alpha}}{}^{(1)}(\mathbf{r},\mathbf{r}';\omega) = -\frac{1}{\omega^2}\left[\chi^{(1)}_{\mathbf{jj}}(\mathbf{r},\mathbf{r}';\omega) - \overset{\leftrightarrow}{\mathbb{1}}\,\rho(\mathbf{r})\delta(\mathbf{r}-\mathbf{r}')\right], \tag{23}$$

where $\chi^{(1)}_{\mathbf{jj}}$ is the current-current response function and ρ is the electronic density of the system. The surface-averaged quasipolarizability is

$$\overset{\leftrightarrow}{\tilde{\alpha}}{}^{(1)S}(\mathbf{q};\omega) = \frac{1}{L_z}\int dz_1 \int dz_2 e^{-iq_z z_1}\mathcal{C}(z_1) \times \overset{\leftrightarrow}{\tilde{\alpha}}_{\mathbf{00}}(\mathbf{q}_{||},z_1,z_2;\omega)e^{iq_z z_2}. \tag{24}$$

Defining $\chi^{(1)S}_{\mathbf{jj}}(\mathbf{q},\mathbf{q};\omega)$ and ρ^S in the same way, we get

$$\overset{\leftrightarrow}{\tilde{\alpha}}{}^{(1)S}(\mathbf{q};\omega) = -\frac{1}{\omega^2}\left[\chi^{(1)S}_{\mathbf{jj}}(\mathbf{q},\mathbf{q};\omega) - \overset{\leftrightarrow}{\mathbb{1}}\langle\rho^S\rangle\right]. \tag{25}$$

Inserting Eq. (25) into Eq. (22), we obtain the longitudinal part of the surface macroscopic dielectric tensor in terms of response functions,

$$\epsilon_M^{S,LL}(\hat{\mathbf{q}};\omega) = 1 - \lim_{\mathbf{q}\to\mathbf{0}} \frac{4\pi}{\omega^2}\frac{\frac{\mathbf{q}}{|\mathbf{q}|}\chi^{(1)S}_{\mathbf{jj}}(\mathbf{q},\mathbf{q};\omega)\frac{\mathbf{q}}{|\mathbf{q}|} - \langle\rho^S\rangle}{1 + v_\mathbf{0}(\mathbf{q})\chi^{(1)}_{\mathbf{00}}(\mathbf{q},\mathbf{q};\omega)}, \tag{26}$$

where $v_\mathbf{0}(\mathbf{q}) = 4\pi/q^2$ is the macroscopic Coulomb potential and $\langle\rho^S\rangle = \langle\rho(\mathbf{r})\mathcal{C}(z)\rangle = \frac{\langle\rho\rangle}{2}$. We used the link between the longitudinal-longitudinal part of the quasipolarizability and the density-density response function $\chi^{(1)}$, as shown in Ref. [30].

To replace the current-current response function $\chi^{(1)S}_{\mathbf{jj}}$ in Eq. (26) by the density-density response function $\chi^{(1)S}$, we use charge conservation in the presence of a cut function, which can be written as (see Appendix B)

$$\omega^2\chi^{(1)S}(\mathbf{k},\mathbf{k}';\omega) = \mathbf{k}\cdot\chi^{(1)S}_{\mathbf{jj}}(\mathbf{k},\mathbf{k}';\omega)\cdot\mathbf{k}' - \langle\rho^S\rangle\delta(\mathbf{k}-\mathbf{k}'). \tag{27}$$

Two restrictions are needed to derive Eq. (27): (i) the cut function $\mathcal{C}(z)$ is a step function, located at the center of the matter (see Fig. 1) and (ii) the slab has a mirror plane perpendicular to the z axis. The consequences are that (i) the slab must be symmetric, with two identical surfaces and (ii) this formalism cannot be used to perform a layer-by-layer analysis, except in the independent-particle approximation.

Note that this choice of the cut function is one of the most used for surface linear [45–47] and second-harmonic generation [36–40] calculations, with an exception for Refs. [34,35], where $\mathcal{C}(z)$ has been chosen as a smoothly varying function.

We finally get an expression for the LL part of the surface dielectric tensor depending only on the density-density response function of the system and its surface average,

$$\epsilon_M^{S,LL}(\hat{\mathbf{q}};\omega) = 1 - \lim_{\mathbf{q}\to\mathbf{0}} v_\mathbf{0}(\mathbf{q})\frac{\chi^{(1)S}_{\mathbf{00}}(\mathbf{q},\mathbf{q};\omega)}{1 + v_\mathbf{0}(\mathbf{q})\chi^{(1)}_{\mathbf{00}}(\mathbf{q},\mathbf{q};\omega)}. \tag{28}$$

This equation is the main result of this section, as the longitudinal part of the surface dielectric tensor is now expressed in terms of quantities that depend only on the electronic density of the system, and can be evaluated in the framework of TDDFT. To obtain this result, we have introduced a quantity, $\chi^{(1)S}$, that will be evaluated explicitly in the next section.

One remarks that if we choose $\mathcal{C}(z)$ to be 1 everywhere, we recover the expression of the LL part of the dielectric function used for bulk materials [48], showing the consistency of our approach. We also note here that $\chi^{(1)S}$ and $\chi^{(1)S}_{\mathbf{jj}}$ are not response functions, but correspond to the surface macroscopic average of the response functions. Nevertheless, for the ease of denomination, we will retain this name.

C. Calculation of $\epsilon_M^{S,LL}$ in TDDFT

The evaluation of Eq. (28) requires the calculation of the two quantities $\chi^{(1)S}(\mathbf{q},\mathbf{q};\omega)$ and $\chi^{(1)}_{\mathbf{00}}(\mathbf{q},\mathbf{q};\omega)$, in the optical limit. While the latter can be computed easily in TDDFT [48], the evaluation of $\chi^{(1)S}(\mathbf{q},\mathbf{q};\omega)$ is more cumbersome. Equation (28) can be rewritten as

$$\epsilon_M^{S,LL}(\hat{\mathbf{q}};\omega) = 1 - \lim_{\mathbf{q}\to\mathbf{0}} v_\mathbf{0}(\mathbf{q}) \times \frac{1}{L_z}\frac{\sum_{G_z}\tilde{\mathcal{C}}(-G_z)\chi^{(1)}_{\mathbf{G}_z\mathbf{0}}(\mathbf{q},\mathbf{q};\omega)}{1 + v_\mathbf{0}(\mathbf{q})\chi^{(1)}_{\mathbf{00}}(\mathbf{q},\mathbf{q};\omega)}, \tag{29}$$

where $\tilde{\mathcal{C}}$ is the Fourier transform of the cut function $\mathcal{C}(z)$.

From now on, we assume the random-phase approximation (RPA). Within TDDFT, this approximation amounts to neglecting the exchange correlation in the response, i.e., excitonic effects [49,50]. The response function of the fully interacting system $\chi^{(1)}$ is then related to the Kohn-Sham response function $\chi_0^{(1)}$ of the system through a Dyson-like equation [48],

$$\chi^{(1)}_{\mathbf{GG}'} = \chi^{(1)}_{0,\mathbf{GG}'} + \sum_{\mathbf{G}_1}\chi^{(1)}_{0,\mathbf{GG}_1}v_{\mathbf{G}_1}\chi^{(1)}_{\mathbf{G}_1\mathbf{G}'}, \tag{30}$$

where $v_{\mathbf{G_1}} = 4\pi/|\mathbf{q}+\mathbf{G_1}|^2$ corresponds to the Fourier transform of the Coulomb potential. For brevity, we omitted the $\mathbf{q}$ and frequency dependence.

It is convenient to introduce $\bar{\chi}$, the response function to the total macroscopic classical potential $v_{\mathbf{0}}$, defined by [51]

$$\chi^{(1)}_{\mathbf{GG}'} = \bar{\chi}^{(1)}_{\mathbf{GG}'} + \bar{\chi}^{(1)}_{\mathbf{G0}} v_{\mathbf{0}} \chi^{(1)}_{\mathbf{0G}'}, \tag{31}$$

which implies that

$$\bar{\chi}^{(1)}_{\mathbf{GG}'} = \chi^{(1)}_{0,\mathbf{GG}'} + \sum_{\mathbf{G_1}} \chi^{(1)}_{0,\mathbf{GG_1}} \bar{v}_{\mathbf{G_1}} \bar{\chi}^{(1)}_{\mathbf{G_1G}'}, \tag{32}$$

where $\bar{v}_{\mathbf{G}}(\mathbf{q}) = v_{\mathbf{G}}(\mathbf{q})$ if $\mathbf{G} \neq \mathbf{0}$, and 0 if $\mathbf{G} = \mathbf{0}$.

From Eq. (31), we obtain directly that $\bar{\chi}^{(1)}_{\mathbf{G0}} = \frac{\chi^{(1)}_{\mathbf{G0}}}{1+v_{\mathbf{0}}\chi^{(1)}_{\mathbf{00}}}$, leading to

$$\epsilon^{S,LL}_{M}(\hat{\mathbf{q}};\omega) = 1 - \lim_{\mathbf{q}\to\mathbf{0}} v_{\mathbf{0}}(\mathbf{q}) \bar{\chi}^{(1)S}_{\mathbf{00}}(\mathbf{q},\mathbf{q};\omega). \tag{33}$$

The analog of Eq. (33) has been previously derived for the bulk dielectric function $\epsilon^{LL}_M(\hat{\mathbf{q}};\omega)$ (see Ref. [51]), but here we show that it is also possible to use the $\bar{\chi}^{(1)}$ function for the surface dielectric tensor.

Applying surface macroscopic averaging to Eq. (32), we obtain the definition of $\bar{\chi}^{(1)S}_{\mathbf{00}}(\mathbf{q},\mathbf{q};\omega)$ through the equation

$$\begin{aligned}\bar{\chi}^{(1)S}_{\mathbf{00}}(\mathbf{q},\mathbf{q};\omega) = \chi^{(1)S}_{0,\mathbf{00}}(\mathbf{q},\mathbf{q};\omega) + \sum_{\mathbf{G_1}\neq\mathbf{0}} \chi^{(1)S}_{0,\mathbf{0G_1}} \\ \times (\mathbf{q},\mathbf{q};\omega) v_{\mathbf{G_1}}(\mathbf{q}) \bar{\chi}^{(1)}_{\mathbf{G_1}0}(\mathbf{q},\mathbf{q};\omega).\end{aligned} \tag{34}$$

The derivation and the expression of $\chi^{(1)S}_0$ are given in Appendix C. We solve the Dyson equation for $\bar{\chi}^{(1)}$ [Eq. (32)] and then use Eq. (34) to get $\bar{\chi}^{(1)S}_{\mathbf{00}}(\mathbf{q},\mathbf{q};\omega)$.

We emphasize that this result allows us to describe how a surface affects the optical response of a material, with the convenience and efficiency of a supercell calculation, assuming that the slab is thick enough to correctly describe the surface region.

IV. MACROSCOPIC SECOND-ORDER TENSOR OF CRYSTAL SURFACES

We now turn to the evaluation of the macroscopic surface second-order response function, giving access to second-harmonic generation, following the approach used for the surface dielectric tensor.

A. Surface average of $\chi^{(2)}$

The in-plane averaged macroscopic second-order susceptibility tensor is defined by

$$\begin{aligned}&\mathbf{D}^{(2)}_{\mathbf{0}}(\mathbf{q}_{||},z;\omega)\\ &\quad= 4\pi \int d\omega_1 d\omega_2 \delta(\omega-\omega_1-\omega_2) \int dz_1 dz_2\\ &\qquad\times \sum_{\mathbf{q_1q_2}} \delta_{\mathbf{q},(\mathbf{q_1}+\mathbf{q_2})} \chi^{(2)}_m(\mathbf{q}_{||},z,\mathbf{q_1}_{||},z_1,\mathbf{q_2}_{||},z_2;\omega_1,\omega_2)\\ &\qquad\times \mathbf{E_0}(\mathbf{q_1}_{||},z_1;\omega_1)\mathbf{E_0}(\mathbf{q_2}_{||},z_2;\omega_2),\end{aligned} \tag{35}$$

and using the expression of $\mathbf{D}^{(2)}$ given in Eq. (16), for $\mathbf{G}_{||} = 0$, we obtain

$$\begin{aligned}&\chi^{(2)}_m(\mathbf{q}_{||},z,\mathbf{q_1}_{||},z_1,\mathbf{q_2}_{||},z_2;\omega_1,\omega_2)\\ &\quad= \frac{1}{2L_z} \sum_{q_zG_z} e^{i(q_z+G_z)z} \sum_{q_{z1}q_{z2}} \delta_{q_z,(q_{z1}+q_{z2})}\\ &\qquad\times\left[\frac{4\pi \overleftrightarrow{\tilde{\alpha}}^{(1)}_{\mathbf{G0}}(\mathbf{q},\mathbf{q};\omega)\frac{\mathbf{q}}{|\mathbf{q}|}\frac{\mathbf{q}}{|\mathbf{q}|}}{1-4\pi\tilde{\alpha}^{LL}_{\mathbf{00}}(\mathbf{q},\mathbf{q};\omega)} \overleftrightarrow{\tilde{\alpha}}^{(2)}_{\mathbf{000}}(\mathbf{q},\mathbf{q_1},\mathbf{q_2};\omega_1,\omega_2)\right.\\ &\qquad\left.+ \overleftrightarrow{\tilde{\alpha}}^{(2)}_{\mathbf{G_z00}}(\mathbf{q},\mathbf{q_1},\mathbf{q_2};\omega_1,\omega_2)\right] e^{-iq_{z1}z_1} e^{-iq_{z2}z_2} \overleftrightarrow{A}\\ &\qquad\times (\mathbf{q_1};\omega_1) \overleftrightarrow{A}(\mathbf{q_2};\omega_2).\end{aligned} \tag{36}$$

The surface macroscopic second-order response function is defined as

$$\begin{aligned}&\chi^{(2)S}_M(\mathbf{q},\mathbf{q_1},\mathbf{q_2};\omega_1,\omega_2)\\ &\quad= \frac{1}{2L_z^2} \int dz dz_1 dz_2 e^{-iq_z z} \mathcal{C}(z)\\ &\qquad\times \chi^{(2)}_m(\mathbf{q}_{||},z,\mathbf{q_1}_{||},z_1,\mathbf{q_2}_{||},z_2;\omega_1,\omega_2) e^{iq_{z1}z_1} e^{iq_{z2}z_2},\end{aligned} \tag{37}$$

where $\mathcal{C}(z)$ is the same cut function as the one introduced in Sec. III. This quantity describes the second-order response of a single surface of a slab in supercell geometry.

Performing the spatial integration, one finally gets

$$\begin{aligned}&\chi^{(2)S}_M(\mathbf{q},\mathbf{q_1},\mathbf{q_2};\omega_1,\omega_2)\\ &\quad= \left[\frac{4\pi \overleftrightarrow{\tilde{\alpha}}^{(1)S}(\mathbf{q};\omega)\frac{\mathbf{q}}{|\mathbf{q}|}\frac{\mathbf{q}}{|\mathbf{q}|}}{1-4\pi\tilde{\alpha}^{LL}_{\mathbf{00}}(\mathbf{q},\mathbf{q};\omega)} \overleftrightarrow{\tilde{\alpha}}^{(2)}_{\mathbf{000}}(\mathbf{q},\mathbf{q_1},\mathbf{q_2};\omega_1,\omega_2)\right.\\ &\qquad\left.+ \overleftrightarrow{\tilde{\alpha}}^{(2)S}(\mathbf{q},\mathbf{q_1},\mathbf{q_2};\omega_1,\omega_2)\right] \overleftrightarrow{A}(\mathbf{q_1};\omega_1) \overleftrightarrow{A}(\mathbf{q_2};\omega_2).\end{aligned} \tag{38}$$

This equation is the equivalent of Eq. (21) for the second order, where both the bulk quasipolarizability ($\overleftrightarrow{\tilde{\alpha}}^{(2)}$) and its surface counterpart ($\overleftrightarrow{\tilde{\alpha}}^{(2)S}$) contribute.

B. Optical limit for the surface macroscopic second-order susceptibility

Similarly to the linear case, we now consider the optical limit and calculate the longitudinal (LLL) part of the macroscopic second-order susceptibility tensor.

We obtain, from charge conservation in the presence of the cut function and with the same restrictions as for the linear response [see Eq. (B5)],

$$\begin{aligned}&\overleftrightarrow{\tilde{\alpha}}^{(2)S,LLL}(\mathbf{q},\mathbf{q_1},\mathbf{q_2};\omega_1,\omega_2)\\ &\quad= \frac{-i}{2|\mathbf{q}||\mathbf{q_1}||\mathbf{q_2}|} \chi^{(2)S}_{\mathbf{000}}(\mathbf{q},\mathbf{q_1},\mathbf{q_2};\omega_1,\omega_2),\end{aligned} \tag{39}$$

where $\chi^{(2)}$ is the density-density-density response function. The LLL part of the macroscopic-surface second-order susceptibility tensor reads

$$\chi_M^{(2)S,LLL}(\mathbf{q},\mathbf{q_1},\mathbf{q_2};\omega_1,\omega_2) = \frac{-i}{2|\mathbf{q}||\mathbf{q_1}||\mathbf{q_2}|} \times\big[-v_\mathbf{0}(\mathbf{q})\bar{\chi}_{\mathbf{00}}^{(1)S}(\mathbf{q},\mathbf{q};\omega)\chi_{\mathbf{000}}^{(2)}(\mathbf{q},\mathbf{q_1},\mathbf{q_2};\omega_1,\omega_2) +\chi_{\mathbf{000}}^{(2)S}(\mathbf{q},\mathbf{q_1},\mathbf{q_2};\omega_1,\omega_2)\big]\epsilon_M^{LL}(\mathbf{q_1};\omega_1)\epsilon_M^{LL}(\mathbf{q_2};\omega_2). \quad (40)$$

It shows that the LLL part of the surface second-order susceptibility tensor depends only on the density-density-density response function and its surface average. This equation is the equivalent of Eq. (28) obtained for the linear case. We also have to make the link between the second-order surface quantity $\chi^{(2)S}$ and the second-order response function $\chi^{(2)}$, as obtained in TDDFT.

C. Calculation of $\chi_M^{(2)S,LLL}$ in TDDFT

Similarly to the linear case, we define $\bar{\chi}^{(2)}$ as the second-order response function to the total macroscopic classical potential and we have shown (see Appendix D) that $\chi^{(2)}$ can be expressed in terms of $\bar{\chi}^{(2)}$ as

$$\chi_{\mathbf{GG'G''}}^{(2)} = \bar{\chi}_{\mathbf{G0}}^{(1)}v_\mathbf{0}\chi_{\mathbf{0G'G''}}^{(2)} + \sum_{\mathbf{G_1G_2}}\bar{\chi}_{\mathbf{GG_1G_2}}^{(2)}\big[\delta_{\mathbf{G_1,G'}}+\delta_{\mathbf{G_1,0}}v_\mathbf{0}\chi_{\mathbf{0G'}}^{(1)}\big] \times\big[\delta_{\mathbf{G_2,G''}}+\delta_{\mathbf{G_2,0}}v_\mathbf{0}\chi_{\mathbf{0G''}}^{(1)}\big], \quad (41)$$

and we obtain, from surface macroscopic averaging, that

$$\chi_{\mathbf{000}}^{(2)S} = \bar{\chi}_{\mathbf{00}}^{(1)}v_\mathbf{0}\chi_{\mathbf{000}}^{(2)} + \bar{\chi}^{(2)S}\big[1+v_\mathbf{0}\chi_{\mathbf{00}}^{(1)}\big]\big[1+v_\mathbf{0}\chi_{\mathbf{00}}^{(1)}\big]. \quad (42)$$

The quantity $\bar{\chi}^{(2)S}$ is given in RPA by (see Appendix D)

$$\bar{\chi}_{\mathbf{000}}^{(2)S} = \sum_{\mathbf{G1}}\chi_{0,\mathbf{0G_1}}^{(1)S}\bar{v}_{\mathbf{G_1}}\bar{\chi}_{\mathbf{G_100}}^{(2)} + \sum_{\mathbf{G_1G_2}}\chi_{0\mathbf{0G_1G_2}}^{(2)S}\big[\delta_{\mathbf{G_10}}+\bar{v}_{\mathbf{G_1}}\bar{\chi}_{\mathbf{G_10}}\big]\big[\delta_{\mathbf{G_20}}+\bar{v}_{\mathbf{G_2}}\bar{\chi}_{\mathbf{G_20}}\big]. \quad (43)$$

Inserting Eq. (42) into Eq. (40) yields

$$\chi_M^{(2)S,LLL}(\mathbf{q},\mathbf{q_1},\mathbf{q_2};\omega_1,\omega_2) = \frac{-i}{2|\mathbf{q}||\mathbf{q_1}||\mathbf{q_2}|}\bar{\chi}_{\mathbf{000}}^{(2)S}(\mathbf{q},\mathbf{q_1},\mathbf{q_2};\omega_1,\omega_2). \quad (44)$$

This equation is the second-order equivalent of Eq. (33), where we find that the surface macroscopic quantity can be obtained from the surface response function to the total macroscopic classical potential. This exhibits the tight relation between the macroscopic quantities and the response functions to the total macroscopic classical potential ($\bar{\chi}$). Indeed, it was already known that the bulk linear optical properties (ϵ_M) were given by either the response to the total potential ($\chi^{(1)}$) or by the response to the total macroscopic classical potential ($\bar{\chi}^{(1)}$). Here we generalize this result by showing that the nonlinear optical properties of bulk ($\chi_M^{(2)}$) and surfaces ($\chi_M^{(2)S}$) can also be obtained from the response functions to the total macroscopic classical potential. We have transformed the problem of computing $\chi_M^{(2)S,LLL}$ into the problem of computing $\bar{\chi}_{\mathbf{000}}^{(2)S}$, given by

$$\bar{\chi}_{\mathbf{000}}^{(2)S}(\mathbf{q},\mathbf{q_1},\mathbf{q_2};\omega) = \sum_{\mathbf{G1}}\chi_{0,\mathbf{0G_1}}^{(1)S}(\mathbf{q};\omega)\bar{v}_{\mathbf{G_1}}(\mathbf{q})\bar{\chi}_{\mathbf{G_100}}^{(2)}(\mathbf{q},\mathbf{q_1},\mathbf{q_2};\omega) + \sum_{\mathbf{G_1G_2}}\chi_{0,\mathbf{0G_1G_2}}^{(2)S}(\mathbf{q},\mathbf{q_1},\mathbf{q_2};\omega)\big[\delta_{\mathbf{G_10}}+\bar{v}_{\mathbf{G_1}}(\mathbf{q_1})\bar{\chi}_{\mathbf{G_10}}^{(1)}(\mathbf{q_1};\omega)\big] \times\big[\delta_{\mathbf{G_20}}+\bar{v}_{\mathbf{G_2}}(\mathbf{q_2})\bar{\chi}_{\mathbf{G_20}}^{(1)}(\mathbf{q_2};\omega)\big]. \quad (45)$$

The derivation of $\chi_0^{(2)S}$ is similar to $\chi_0^{(1)S}$ (see Appendix C). We solve the Dyson equation for $\bar{\chi}^{(2)}$ [Eq. (D9)] and then use Eq. (45) to get $\bar{\chi}^{(2)S}$.

Note that if we put $\mathcal{C}(z)=1$ in Eq. (38), we recover the result for the bulk obtained in Ref. [17], while Eq. (45) gives, in that case, an alternative expression for $\chi_M^{(2)}$.

V. NUMERICAL RESULTS

We have applied this formalism to study the optical properties of silicon surfaces. We have used the recently developed selected-**G** method in order to correctly take into account the LF effect in the supercell calculation [24]. The cut function $\mathcal{C}(z)$ has allowed us to extract the single-surface response for SHG calculations. Before presenting SHG results, we have addressed the question of the independence of the two surfaces in a slab geometry. For this purpose, we have considered the linear case. Results do not rely on $\mathcal{C}(z)$, since we have dealt with asymmetric supercells.

The electronic structure for the ground state was determined within DFT in the local density approximation (LDA), using the plane-wave ABINIT code [52]. We used norm-conserving Troullier-Martins pseudopotentials [53] for Si and H atoms. The linear response calculations are performed using the DP code [54], whereas the SHG calculations where carried out using the 2LIGHT code [55].

A. Independence of the two surfaces in a slab geometry

In the independent-particle approximation, the two surfaces of the slab have been shown to be independent for linear optics [45] and second-harmonic generation [41]. When local-field effects are included, due to the long-range Coulomb interaction, the two surfaces of the slab of matter may potentially couple. In that case, it could be difficult to interpret the result of a slab calculation in terms of the semi-infinite system that we want to model.

To check the independence of the two surfaces, we consider three different slabs (see Fig. 2): two symmetric slabs, composed of (a) clean surfaces and (b) dihydride surfaces, and (c) an asymmetric slab with a clean surface and a dihydride surface.

Results for the linear spectra are presented in Fig. 3. These spectra have been computed for two different sizes of the slab: 12 atomic layers, i.e., 16.29 Å (top panels of Fig. 3), and 16 atomic layers, i.e., 21.72 Å (bottom panels of Fig. 3). These calculations include the local-field effects and have been performed using the selected-**G** method. The local fields do not modify the shape of the spectra. They only lead to a small

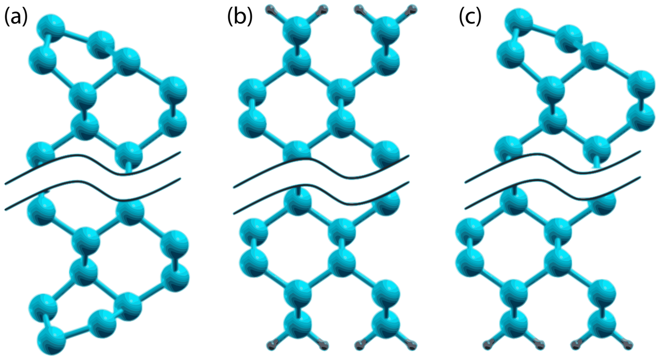

FIG. 2. Ending of the three slabs used: (a) symmetric Clean-Clean, (b) symmetric DiH-DiH, and (c) asymmetric Clean-DiH.

reduction of the amplitude for the in-plane components. For the z component, due to the finite thickness of the slab, the reduction is a bit larger and a small blueshift is also visible [24]. In all cases, we used 256 off-symmetry in-plane $\mathbf{k}$ points. For 12 atomic layers, spectra were obtained using 250 bands and 250 $\mathbf{G}$ vectors, and for 16 atomic layers, we used 300 bands and 300 $\mathbf{G}$ vectors. For both cases, the height of matter and vacuum are equal and we have checked that this amount of vacuum is enough to prevent the coupling between slabs. As stated before, the calculations presented here have been done without the $\mathcal{C}(z)$ cut function. We have checked that for the symmetric slabs, the results are the same when using $\mathcal{C}(z)$.

The spectra denoted "Average" correspond to the half sum of the two symmetric slab spectra. The difference between these spectra and the one obtained for the asymmetric slab ("Clean-DiH") are found to be small for the 12 atomic layers. When increasing the thickness of the slab, the differences almost vanish. The spectra calculated without local field (NLF) yield the same quantitative differences (not shown here) and we conclude that these remaining differences originate from the finite size of the slabs and not from the local fields.

This shows finally that the surfaces in a slab are also independent in the presence of LF, as soon as the slab is thick enough.

B. Components of the surface second-order susceptibility tensor

We calculated the SHG spectra, including the effects of local fields, of the dihydride Si(001)1 × 1:2H [6,15,37,56–61], monohydride Si(001)2 × 1:H [6,60], and clean Si(001)2 × 1 [6,37,59] surfaces.

The calculations are performed for slabs of 24 atomic layers. The convergence parameters are summarized in Table I. The spectra have been obtained using a broadening $\eta =$ 100 meV.

For the Si(001)1 × 1:2H surface, three independent components of the second-order susceptibility tensor are nonzero. The corresponding spectra, with and without local-field effects, are reported in Fig. 4. These three components are also shown for the two other surfaces: monohydride Si(001)2 × 1:H (Fig. 5) and clean Si(001)2 × 1 (Fig. 6). For

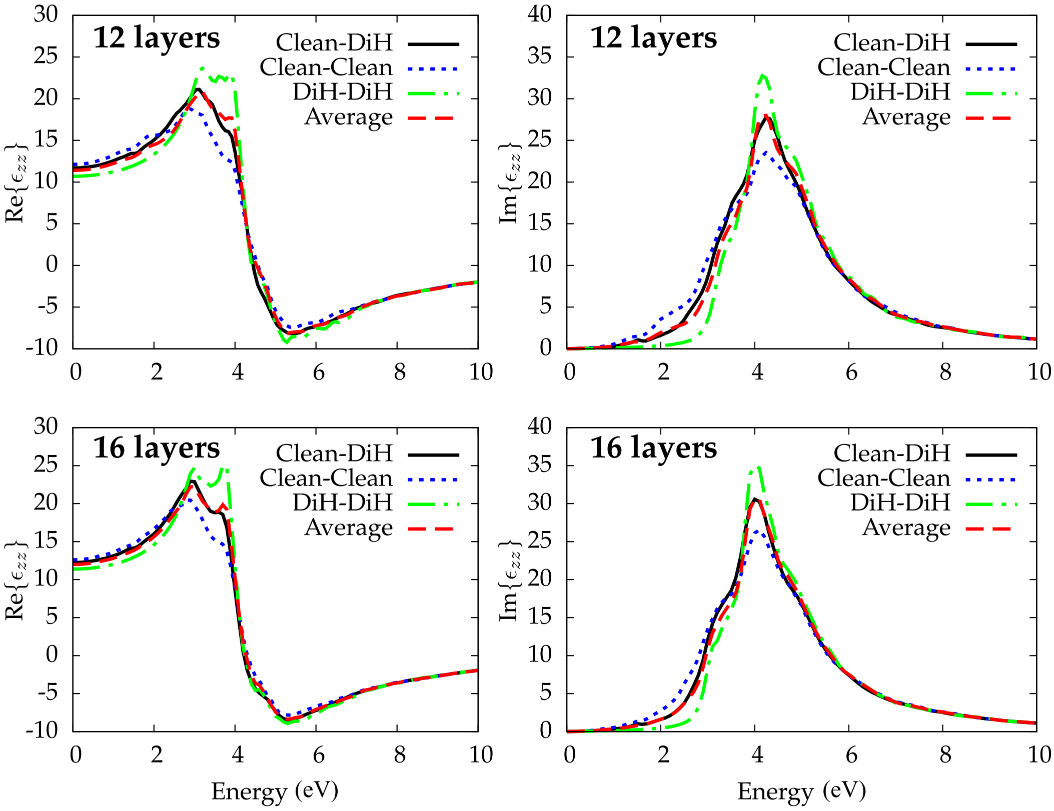

FIG. 3. Comparison between the real part (left panel) and imaginary part (right panel) of ϵ_{zz} computed for two sizes of the slabs (12 layers: top; 16 layers: bottom): Clean-DiH (black solid curve), Clean-Clean (blue dotted curve), DiH-DiH (green dot-dashed curve), and the average of the two symmetric slabs (Average: red dashed curve). Local-field effects are included.

TABLE I. Convergence parameters used for the different Si(001) surfaces: nkpt stands for the number of in-plane off-symmetry **k** points; npw and nband are the number of plane waves and bands, respectively; nmat is the number of **G** vectors used to converge the local field. Note that due to the symmetry, twice fewer atoms are needed for the 2H.

	Si(001)1 × 1:2H	Si(001)2 × 1:H	Si(001)2 × 1
nkpt	288	256	256
npw	3999	3989	3989
nmat	73	93	89
nband	140	220	220

these two last cases, other nonvanishing components can be found, but are not shown here.

For the *yyz* component, the effect of local fields is a slight reduction of the amplitude of the peak (see top panels of Figs. 4–6). For the *zzz* and *zyy* components, the effect is much stronger and results in a blueshift. Indeed, the main structure of the *zzz* component, located at 1.9 eV, appears now at 3.8 eV for the two hydrogenated surfaces, and at 2.6 eV for the clean surface (center panels of Figs. 4–6). The same kind of behavior is seen for the *zyy* component (bottom panels of Figs. 4–6).

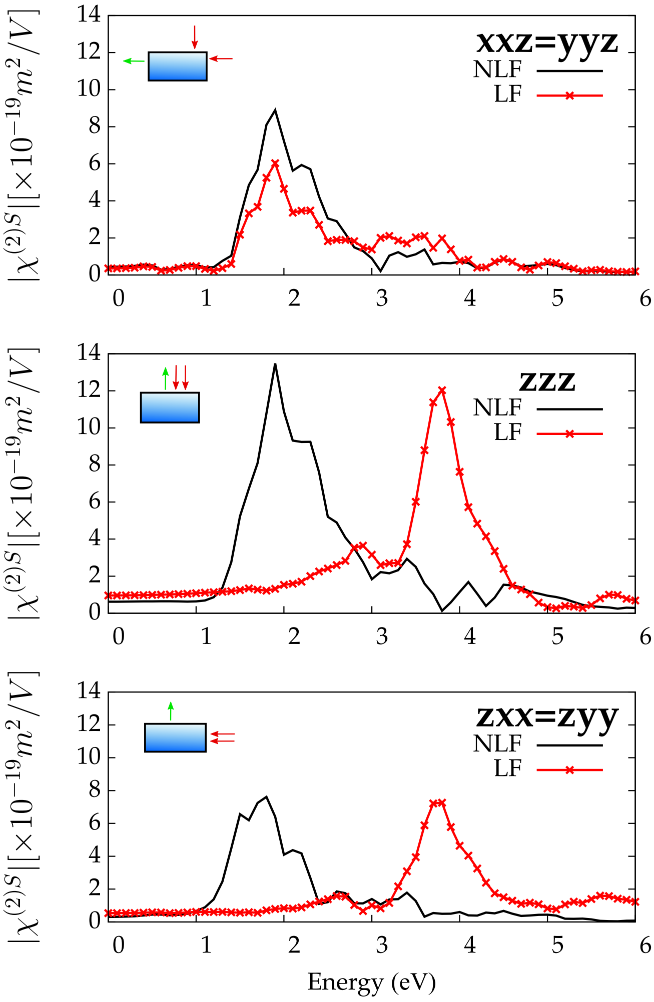

FIG. 4. Surface second-harmonic generation spectra of the dihydride Si(001)1 × 1:2H surface, for the *yyz*, *zzz*, and *zyy* components of the $\chi^{(2)S}$ tensor. No scissor correction is included.

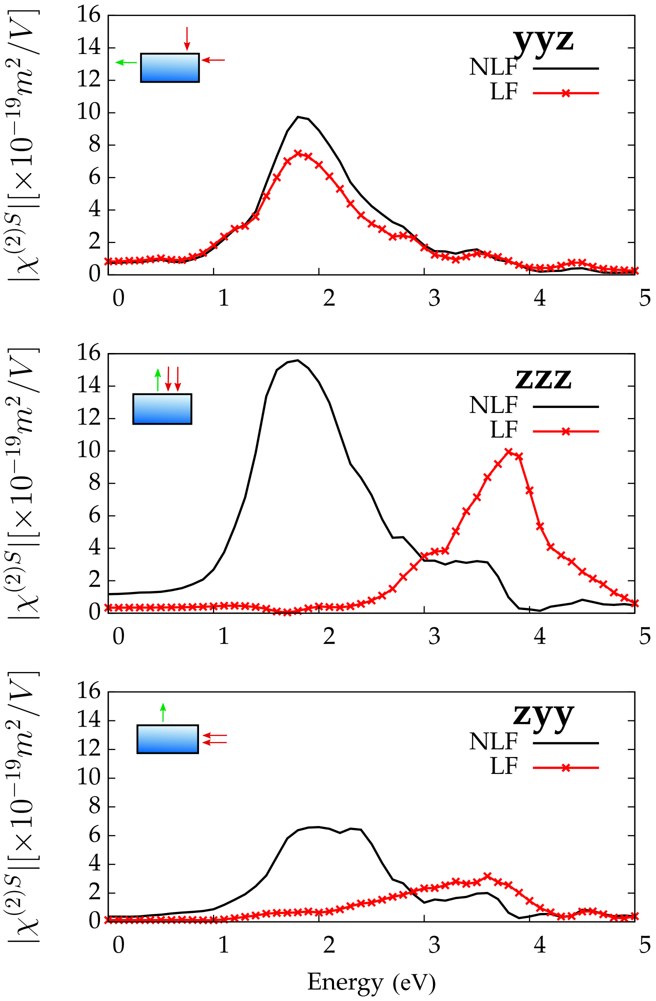

FIG. 5. Surface second-harmonic generation spectra of the monohydride Si(001)2 × 1:H surface, for the *yyz*, *zzz*, and *zyy* components of the $\chi^{(2)S}$ tensor. No scissor correction is included.

A deeper analysis of these effects has been performed on the Si(001)1 × 1:2H. For this purpose, we recall that SHG spectra can present two series of peaks, arising from the different kinds of resonances at ω and 2ω, as shown in Ref. [17]. Screening and many-body effects can be accounted for using a scissor operator [62], which affects differently the peaks coming from the ω or 2ω resonances and discussed in Ref. [41]. To investigate the nature of the shift observed in Figs. 4–6, we have compared the spectra with and without a scissor operator. The scissor correction has been chosen to be $\Delta = 0.6$ eV [63].

The spectra are shown in Fig. 7 for the *zzz* component. The effect of introducing the scissor correction on the NLF spectrum (see the two black curves) is a shift of $\Delta/2 = 0.3$ eV, indicating their 2ω origin. On the other hand, the shift observed for the LFE peaks is $\Delta = 0.6$ eV, indicating their 1ω origin (see red curves with crosses). We conclude that the effect of local fields on the *zzz* component is not a blueshift but a

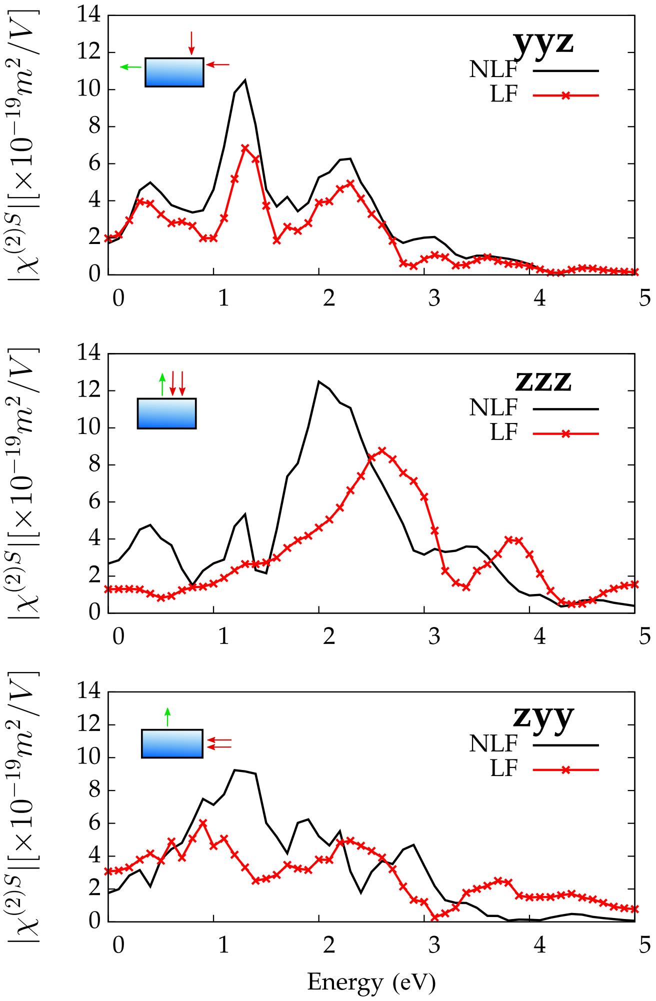

FIG. 6. Surface second-harmonic generation spectra of the clean Si(001)2 × 1 surface, for the *yyz*, *zzz*, and *zyy* components of the $\chi^{(2)S}$ tensor. No scissor correction is included.

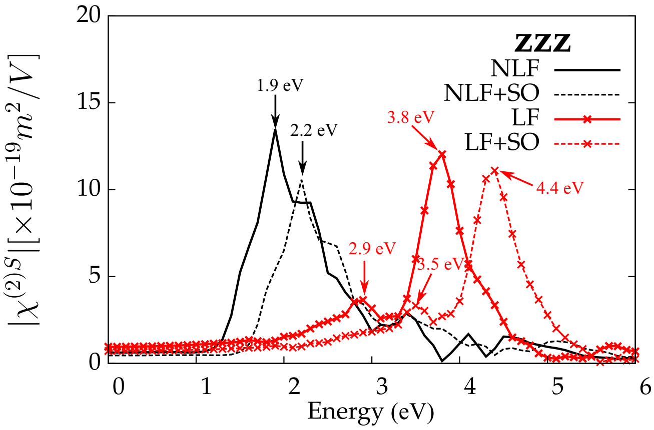

FIG. 7. Comparison of the effect of scissor correction on the surface second-harmonic generation of the Si(001)1 × 1:2H, with (red curves with crosses) and without (black curves without symbols) local fields included. The scissor correction is chosen to be $\Delta = 0.6$ eV. Arrows indicate the positions of main structures.

redistribution of the spectral weight between the 2ω and the 1ω transitions. The same conclusion can be drawn for the other two surfaces. A difference is, however, observed between the clean and the hydrogenated surfaces: the structures are broader for the clean surface, at the origin of the less visible effect.

In many experimental situations, the probed region lies between 1 and 3 eV (see, for instance, Refs. [6,60,64]). Our calculation, including local fields, shows that the spectrum is actually located at higher energy. This is particularly true for the two hydrogenated surfaces (Figs. 4 and 5) and could be at the origin of the experimentally observed "strong quenching" of the spectra for surfaces covered by hydrogen in these energy ranges.

Local fields have different effects, depending on the kind of component studied. If the component corresponds to an emitted polarization propagating perpendicularly to the surface plane (zzz, zxx, and zyy), the spectral weight is redistributed to higher energies by changing the weight from 2ω transitions to 1ω transitions. On the contrary, if the polarization is propagating in the plane of the surface (xxz and yyz), the local fields reduce the spectral weight of the main structures, but their positions are not altered. This result is clearly shown in Figs. 4–6 for the three Si(001) surfaces.

In conclusion, the LFs are found to significantly affect the surface second-harmonic generation, and are therefore required to obtain a quantitative description of the surface second-harmonic generation.

C. Generalized reflection coefficients

The surface susceptibility components enter in the second-harmonic reflection coefficients or generalized reflection coefficients R. They are defined as the ratio of the reflected second-harmonic intensity to the square of the fundamental intensity. They depend on the input and output polarizations, and on the incidence and the azimuthal angles.

The dihydride surface possesses two nonzero reflection coefficients, given by

$$R_{pp}(\theta,\omega) = \frac{2\omega^2 \tan^2\theta}{c^3\epsilon_0} \left| \left| \frac{t^p_{mv}(2\omega)t^p_{vm}(\omega)^2}{\sqrt{\epsilon(2\omega)}\epsilon(\omega)} \frac{q^v_z(2\omega)}{q^m_z(2\omega)} \right|^2 \right| \sin^2\theta\, \chi^{(2)S}_{zzz} + \frac{c^2}{\omega^2}\left[q^m_z(\omega)^2\chi^{(2)S}_{z\|\|} - q^m_z(2\omega)q^m_z(\omega)\chi^{(2)S}_{\|\|z}\right]\Bigg|^2, \tag{46}$$

$$R_{sp}(\theta,\omega) = \frac{2\omega^2 \tan^2\theta}{c^3\epsilon_0} \left| \frac{t^p_{mv}(2\omega)t^s_{vm}(\omega)^2}{\sqrt{\epsilon(2\omega)}} \right|^2 \left| \frac{q^v_z(2\omega)}{q^m_z(2\omega)} \right|^2 \left|\chi^{(2)S}_{z\|\|}\right|^2. \tag{47}$$

θ is the angle of incidence and ϵ is the bulk dielectric function. The subscript $\|$ refers to in-plane directions x or y. t^i_{mv} and t^i_{vm} are the Fresnel transition coefficients, respectively, describing the matter-to-vacuum and the vacuum-to-matter transmissions for the i polarization ($i = p$ or s); see Ref. [65] for more details.

Figure 8 presents the reflection coefficient R_{pp}, corresponding to a p-polarized incoming light and a p-polarized outgoing photon. The difference between the calculations with and without local fields is quite small. This can be understood by the fact that due to the different weights in Eq. (46),

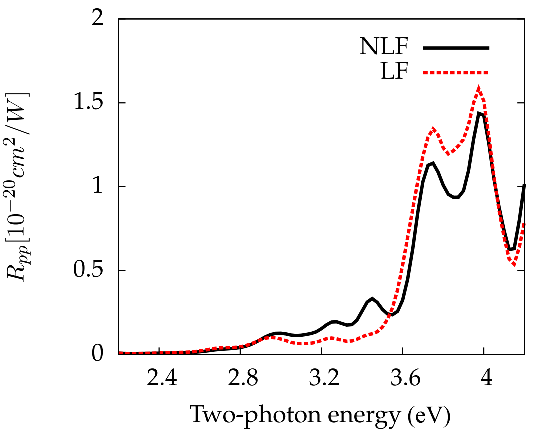

FIG. 8. R_{pp} spectra vs the two-photon energy for an incidence angle $\theta = 45^\circ$ for the dihydride Si(001)1×1:2H surface. The scissor correction is $\Delta = 0.6$ eV. Black solid line: without local-field effects. Red dashed line: with local-field effects.

the R_{pp} spectrum is dominated by the component yyz (as already noticed in Ref. [36]), which is only slightly affected by local-field effects (see Fig. 4).

Figure 9 presents the reflection coefficient R_{sp}, corresponding to an s-polarized incoming light and a p-polarized outgoing photon. Note that the spectrum including local-field (LF) effects is scaled by a factor of 50 to be compared to the one without local fields (NLF). By opposition to the R_{pp} reflection coefficient, the local fields completely quench the response in this energy range. Indeed, the R_{sp} coefficient depends only on $|\chi^{(2)}_{zyy}|$ [see Eq. (47)], which is strongly affected by the local-field effects as seen in Fig. 4.

These results illustrate how local fields can also influence the reflection coefficients due to the mixing of the different second-order components.

D. Comparison with experimental results

We further study second-harmonic generation from the Si(001)1×1:2H surface by comparing our calculations with the experimental results of Ref. [56], in which the spectra for $\chi^{(2)S}_{xxz}$ and $\chi^{(2)S}_{zxx}$ are presented (see Fig. 3, where tensor elements ∂_{31} and ∂_{15} correspond, respectively, to the zxx and xxz components). These results are not given in absolute units but the SHG spectra are normalized with respect to the reflected SHG signal from a quartz reference. However, recently, the absolute amplitude of some components of the surface second-order susceptibility tensor $\chi^{(2)S}$ has been measured [57]. In particular, it was found that $\chi^{(2)S}_{xxz} = 3.5 \pm 0.7 \times 10^{-19}$ m^2/V at the second-harmonic energy $2\omega = 3.1$ eV, for the native-oxide covered Si(001) surface. This energy is out of the resonance due to the E_1 critical point of silicon and is found to be quite insensitive to the surface termination, as shown in Ref. [56]. Using the above value as a reference, we have converted the data of Ref. [56] into absolute units. Due to the uncertainty on the experimental absolute value of $\chi^{(2)S}_{xxz}$ $(3.5 \pm 0.7 \times 10^{-19}\ \mathrm{m}^2/\mathrm{V})$, there is at least 20% of uncertainty on the experimental spectra. Nevertheless, this allows us to compare our calculations with experimental data in absolute units.

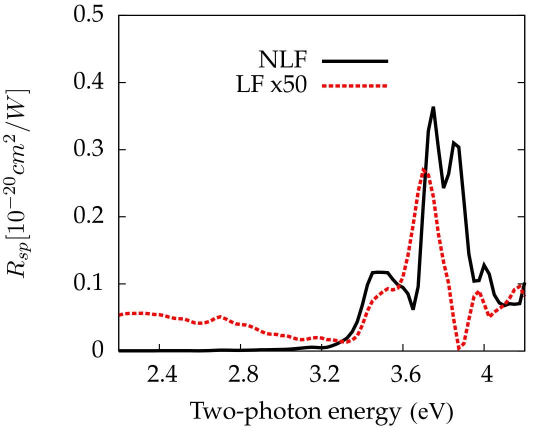

FIG. 9. Same as in Fig. 8, but for the s-in/p-out reflection coefficient R_{sp}.

The comparison between calculations and experimental data is reported in Fig. 10. Due to the small energy range spanned by the experiment, we have decreased the broadening in our calculation (25 meV). It requires that we increase the number of **k** points to 578 for convergence. The value for the scissor operator is $\Delta = 0.6$ eV [66].

The calculation without local fields (left panel of Fig. 10) does not reproduce, even qualitatively, the experimental data, as we found that $|\chi^{(2)}_{zxx}| > |\chi^{(2)}_{xxz}|$ whereas the opposite is observed experimentally; see also Ref. [40]. The local-field effects (center panel of Fig. 10) significantly improves the agreement between theory and experiment. Indeed, the relative weight of the two components is now found to be consistent with the experimental data. Moreover, we obtain a good agreement for the absolute intensity, showing the importance of including local-field effects to quantitatively reproduce the experiments.

Concerning the energy position of the peaks, there is still a discrepancy of about 0.3 eV (in the two-photon energy scale). The experimental data presented here have been measured at room temperature. It is known that the temperature has a strong influence on the peak position of the clean and the monohydride surfaces, and that lowering the temperature induces a blueshift of the E_1 resonance [6,67]. Comparing the SHG spectra of Refs. [6,60,67], we have evaluated that the decrease of the temperature from 300 to 80 K induces a blueshift of about 0.1 eV (in two-photon energy scale), explaining part of the discrepancy. Nevertheless, the effect of the temperature does not entirely explain the difference in the peak positions found here. We would like to stress that including excitonic effects and a GW correction, instead of a scissor operator, would give a much better agreement, as seen in Refs. [63,68]. However, it is beyond the scope of this calculation.

VI. CONCLUSIONS

In this work, we present the detailed derivation of an *ab initio* formalism for the first- and second-order macroscopic optical responses of crystal surfaces, including the local-field effects. We have used a cut function, previously introduced for the independent-particle approximation [41,45,46] to extract the response of a single surface (in a supercell, the two surfaces interfere destructively for the second-order susceptibility), and we have derived an expression of this surface susceptibility to account for local fields.

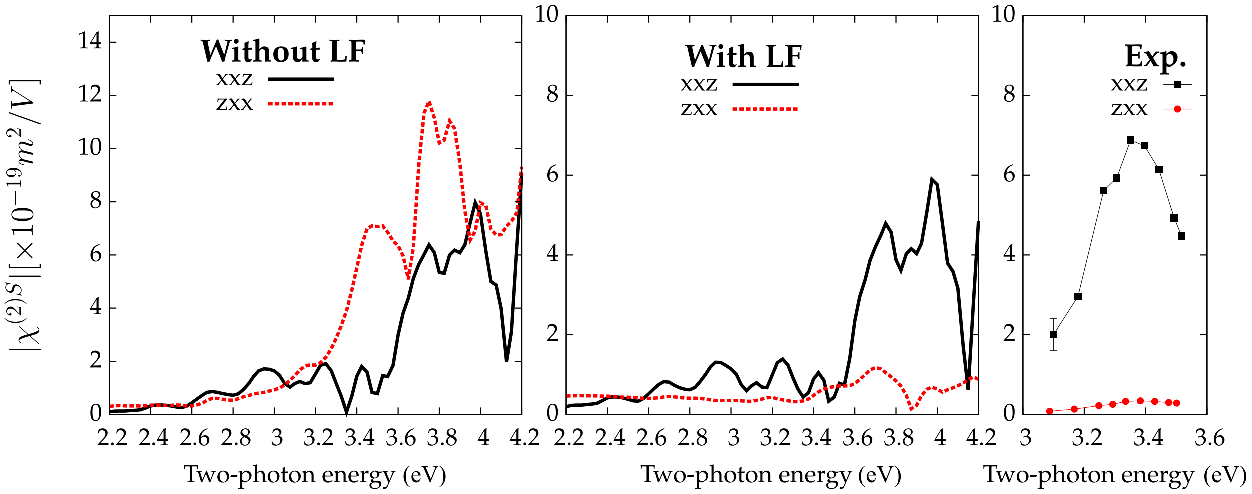

FIG. 10. Comparison between the theoretical calculation of $|\chi^{(2)S}_{xxz}|$ and $|\chi^{(2)S}_{zxx}|$ without local-field effects (left panel), with local-field effects (middle panel), and the experimental data from Ref. [56] (right panel). Here we used $\eta = 0.025$ eV and a scissor correction of $\Delta = 0.6$ eV.

We first established a relation between the macroscopic surface-averaged quantities and the microscopic components of the linear and second-order response functions. In the case of the long-wavelength limit, every quantity can be expressed in terms of the longitudinal response functions, allowing for the use of time-dependent density functional theory. We have shown that they are also related to the response function to the total macroscopic classical potential. Here, this link, which was already known for linear bulk properties, is generalized to nonlinear bulk properties and for surfaces. All of the derivations are done in the framework of the random-phase approximation, but excitonic effects, when they can be accounted for by a scalar exchange-correlation kernel, can be included as a postprocessing [50].

We have applied this formalism to study three silicon surfaces: the dihydride Si(001)1 × 1:2H, the monohydride Si(001)2 × 1:H, and the clean Si(001)2 × 1. We have checked that the two surfaces of a slab are independent, with and without local-field effects. We have evidenced that local fields are particularly important when the emitted electric field is perpendicular to the surface and appears as a blueshift in frequency. Using a scissor operator, we have demonstrated that this apparent shift was indeed a redistribution of the spectral weight between the 2ω and the 1ω transitions. Finally, we have compared our results with experimental data, showing that the inclusion of local-field effects is crucial for a good quantitative agreement.

ACKNOWLEDGMENTS

This work was performed using HPC resources from GENCI-IDRIS Grant No. 090544 and CCRT-DSM Grant No. 100. We would like to thank B. S. Mendoza and S. M. Anderson for helpful discussions.

APPENDIX A: FOURIER TRANSFORM IN THE MIXED SPACE

We define the mixed space as a slab-adapted space where the in-plane periodicity is treated in the reciprocal space and the aperiodic z direction is treated in real space.

The direct and inverse Fourier transforms in this mixed space are defined as

$$f(\mathbf{q}+\mathbf{G}) = \int dz\, e^{-i(q_z+G_z)z} f(\mathbf{q}_{||}+\mathbf{G}_{||},z), \tag{A1}$$

$$f(\mathbf{q}_{||}+\mathbf{G}_{||},z) = \frac{1}{2L_z}\sum_{q_z}^{\mathrm{BZ}}\sum_{G_z} e^{i(q_z+G_z)z} f(\mathbf{q}+\mathbf{G}), \tag{A2}$$

where $\mathbf{q}$ is a vector in the first Brillouin zone, $\mathbf{G}$ is a reciprocal lattice vector, $\mathbf{q} = \mathbf{q}_{||} + q_z\hat{\mathbf{z}}$, $\mathbf{G} = \mathbf{G}_{||} + G_z\hat{\mathbf{z}}$, and $2L_z$ is the size of the cell along the z axis.

For two-variable response functions, one has

$$\chi_{\mathbf{G}_{||1},\mathbf{G}_{||2}}(\mathbf{q}_{||},z_1,z_2) = \frac{1}{2L_z}\sum_{q_z}^{\mathrm{BZ}}\sum_{G_{z1},G_{z2}} e^{i(q_z+G_{z1})z_1} \times \chi_{\mathbf{G}_1,\mathbf{G}_2}(\mathbf{q}) e^{-i(q_z+G_{z2})z_2}, \tag{A3}$$

$$\chi_{\mathbf{G}_1,\mathbf{G}_2}(\mathbf{q}) = \frac{1}{2L_z}\int dz_1 dz_2\, e^{-i(q_z+G_{z1})z_1} \times \chi_{\mathbf{G}_{||1},\mathbf{G}_{||2}}(\mathbf{q}_{||},z_1,z_2) e^{i(q_z+G_{z2})z_2}. \tag{A4}$$

Similar Fourier transform can be written between the mixed space and the real space.

APPENDIX B: CHARGE CONSERVATION AND CUT FUNCTION

Define $\rho^S(\mathbf{r};\omega)$ by $\mathcal{C}(z)\rho(\mathbf{r};\omega)$ and $\mathbf{j}^S_{\mathrm{ind}}(\mathbf{r};\omega)$ by $\mathcal{C}(z)\mathbf{j}_{\mathrm{ind}}(\mathbf{r};\omega)$, where ρ is the density, $\mathbf{j}_{\mathrm{ind}}$ is the induced current, and $\mathcal{C}(z)$ is the cut function used to select the response from a part of the system.

Using vector calculus relations, one can write that

$$\nabla\cdot\left[\mathbf{j}^S_{\mathrm{ind}}(\mathbf{r};\omega)\right] = \mathcal{C}(z)\nabla\cdot[\mathbf{j}_{\mathrm{ind}}(\mathbf{r};\omega)] + \mathbf{grad}\,\mathcal{C}(z)\cdot\mathbf{j}_{\mathrm{ind}}(\mathbf{r};\omega). \tag{B1}$$

Inserting the continuity relation yields

$$\nabla \cdot \left[\mathbf{j}^S_{\text{ind}}(\mathbf{r};\omega)\right] = -i\omega\rho^S(\mathbf{r};\omega) + \mathbf{grad}\mathcal{C}(z)\cdot\mathbf{j}_{\text{ind}}(\mathbf{r};\omega). \quad \text{(B2)}$$

Here we choose to assume the following:

Approximation 1. The system is invariant under the inversion $z \leftrightarrow -z$.

Approximation 2. The function $\mathcal{C}(z)$ is a step function.

Using Approximation 2, one finds that

$$\begin{aligned}\mathbf{grad}\mathcal{C}(z)\cdot\mathbf{j}_{\text{ind}}(\mathbf{r};\omega) &= \hat{\mathbf{e}}_z\cdot\mathbf{j}_{\text{ind}}(\mathbf{r};\omega)\delta(z)\\ &= \hat{\mathbf{e}}_z\cdot\mathbf{j}_{\text{ind}}(x,y,z=0;\omega).\end{aligned}$$

Due to Approximation 1, the plane $z = 0$ is a mirror plane of the system, imposing that $\mathbf{j}_{\text{ind}}$ is contained in the plane $[x,y]$. This results in

$$\mathbf{k}\cdot\mathbf{j}^S_{\text{ind}}(\mathbf{k};\omega) = \omega\rho^S_{\text{ind}}(\mathbf{k};\omega). \quad \text{(B3)}$$

Physically, this result shows that the charge is conserved in each half of the system separately.

Replacing the current and the density by their expressions in terms of response functions [44], we obtain, at first order and second order,

$$\omega^2\chi^{(1)S}(\mathbf{k},\mathbf{k}';\omega) = \mathbf{k}\chi^{(1)S}_{\mathbf{jj}}(\mathbf{k},\mathbf{k}';\omega)\mathbf{k}' - \langle\rho^S\rangle\delta_{\mathbf{k},\mathbf{k}'}k^2, \quad \text{(B4)}$$

$$\omega^3\chi^{(2)S}(\mathbf{k},\mathbf{k}',\mathbf{k}'';\omega) = \mathbf{k}\chi^{(2)S}_{\mathbf{jjj}}(\mathbf{k},\mathbf{k}',\mathbf{k}'';\omega)\mathbf{k}'\mathbf{k}''. \quad \text{(B5)}$$

APPENDIX C: EXPRESSIONS OF $\chi_0^{(1)S}$ AND $\chi_0^{(2)S}$

The elements $\chi_0^{(1)S}(\mathbf{q},\mathbf{q}+\mathbf{G}';\omega)$ are obtained from the independent-particle response function by

$$\chi_0^{(1)S}(\mathbf{q},\mathbf{q}+\mathbf{G}';\omega) = \frac{1}{L_z}\sum_{G_z}\tilde{\mathcal{C}}(-G_z)\left[\chi_0^{(1)}(\mathbf{q};\omega)\right]_{\mathbf{G_z},\mathbf{G}'}, \quad \text{(C1)}$$

where the supercell contains N atomic layers of thickness L_z. Inserting the expression of the Kohn-Sham response function [48] into Eq. (C1), we obtain

$$\chi_0^{(1)S}(\mathbf{q},\mathbf{q}+\mathbf{G}';\omega) = \frac{2}{N_{\mathbf{k}}V_{\text{cell}}}\sum_{n,n'}\sum_{\mathbf{k}}^{BZ}(f_{n,\mathbf{k}} - f_{n',\mathbf{k}+\mathbf{q}})\frac{\tilde{\rho}^S_{n,n',\mathbf{k}}(\mathbf{q})\langle n',\mathbf{k}+\mathbf{q}|e^{i(\mathbf{q}+\mathbf{G}')\mathbf{r}}|n,\mathbf{k}\rangle}{(E_{n,\mathbf{k}} - E_{n',\mathbf{k}+\mathbf{q}} + \omega + i\eta)}, \quad \text{(C2)}$$

where $f_{n,\mathbf{k}}$ is the Fermi occupation number of the Bloch state $|n,\mathbf{k}\rangle$ and

$$\tilde{\rho}^S_{n,n',\mathbf{k}}(\mathbf{q}) = \frac{1}{L_z}\sum_{G_z}\tilde{\mathcal{C}}(-G_z)\langle n,\mathbf{k}|e^{-i(\mathbf{q}+\mathbf{G_z})\mathbf{r}}|n',\mathbf{k}+\mathbf{q}\rangle.$$

This quantity has to be evaluated in the optical limit, $\mathbf{q} \to \mathbf{0}$.

The expression of $\tilde{\rho}^S_{n,n',\mathbf{k}}(\mathbf{q})$ is also given by

$$\tilde{\rho}^S_{n,n',\mathbf{k}}(\mathbf{q}) = \int d^3\mathbf{r}\phi^*_{n,\mathbf{k}}(\mathbf{r})\mathcal{C}(z)e^{-i\mathbf{qr}}\phi_{n,\mathbf{k}+\mathbf{q}}(\mathbf{r}). \quad \text{(C3)}$$

In the optical limit, $\mathbf{q} \to 0$ and therefore, from $\mathbf{k}\cdot\mathbf{p}$ perturbation theory [69], we get

$$\tilde{\rho}^S_{n,n',\mathbf{k}}(\mathbf{q}\to 0) = \langle n,\mathbf{k}|\mathcal{C}(z)|n',\mathbf{k}\rangle + \sum_{m\notin D_{n'}}\frac{\langle n,\mathbf{k}|\mathcal{C}(z)|m,\mathbf{k}\rangle\langle m,\mathbf{k}|\mathbf{qv}|n',\mathbf{k}\rangle}{E_{n',\mathbf{k}} - E_{m,\mathbf{k}}}. \quad \text{(C4)}$$

Using the interband part [70] $\mathbf{r_e}$ of the position operator $\mathbf{r}$, defined by

$$\langle n,\mathbf{k}|\mathbf{r_e}|m,\mathbf{k}'\rangle = (1-\delta_{nm})\delta(\mathbf{k}-\mathbf{k}')\xi_{nm},$$

with $\xi_{nm} = \langle n,\mathbf{k}|\mathbf{r}|m,\mathbf{k}\rangle$ for $m \notin \mathcal{D}_n$, where $\mathcal{D}_n$ are the n-degenerate states, we get

$$\tilde{\rho}^S_{n,n',\mathbf{k}}(\mathbf{q}\to 0) = \langle n,\mathbf{k}|\mathcal{C}(z) - i\mathcal{C}(z)\mathbf{q}\mathbf{r_e}|n',\mathbf{k}\rangle. \quad \text{(C5)}$$

For $n' \notin \mathcal{D}_n$, we have

$$i\langle n,\mathbf{k}|[H,\mathbf{r_e}]|n',\mathbf{k}'\rangle = \langle n,\mathbf{k}|\mathbf{v}|n',\mathbf{k}'\rangle. \quad \text{(C6)}$$

From this result, we can compute the last term of Eq. (C5) for $n' \notin \mathcal{D}_n$,

$$-i\,(E_{n,\mathbf{k}} - E_{n',\mathbf{k}})\langle n,\mathbf{k}|\mathcal{C}(z)\mathbf{r_e}|n',\mathbf{k}\rangle = \langle n,\mathbf{k}|\frac{\mathcal{C}(z)\mathbf{v} + \mathbf{v}\mathcal{C}(z)}{2}|n',\mathbf{k}\rangle. \quad \text{(C7)}$$

Here we recognize the expression of the modified velocity [41], defined by $\boldsymbol{\mathcal{V}} = \frac{\mathcal{C}(z)\mathbf{v}+\mathbf{v}\mathcal{C}(z)}{2}$, which has been previously used to compute surface SHG at the level of the independent-particle approximation.

The final expression of $\tilde{\rho}^S_{n,n',\mathbf{k}}(\mathbf{q}\to 0)$ is

$$\tilde{\rho}^S_{n,n',\mathbf{k}}(\mathbf{q}\to\mathbf{0}) = \langle n,\mathbf{k}|\mathcal{C}(z)|n',\mathbf{k}\rangle + \frac{\langle n,\mathbf{k}|\mathbf{q}\cdot\boldsymbol{\mathcal{V}}|n',\mathbf{k}\rangle}{E_{n,\mathbf{k}} - E_{n',\mathbf{k}}}. \quad \text{(C8)}$$

For $\mathbf{G}' = \mathbf{0}$, and in the limit $\mathbf{q} \to \mathbf{0}$, $\chi_0^{(1)S}$ reads

$$\chi_0^{(1)S}(\mathbf{q},\mathbf{q};\omega) = \frac{2}{N_{\mathbf{k}} V_{\text{cell}}} \sum_{n,n'} \sum_{\mathbf{k}}^{\text{BZ}} f_{nn'} \Bigg[\frac{\langle n,\mathbf{k}|\mathcal{C}(z)|n',\mathbf{k}\rangle \langle n',\mathbf{k}|i\mathbf{q}\cdot\mathbf{r}|n,\mathbf{k}\rangle \langle n',\mathbf{k}|\mathbf{q}\cdot\mathbf{v}|n',\mathbf{k}\rangle}{(E_{n,\mathbf{k}} - E_{n',\mathbf{k}} + \omega + i\eta)^2} + \frac{\langle n,\mathbf{k}|\mathcal{C}(z)|n',\mathbf{k}\rangle \langle n',\mathbf{k}|i\mathbf{q}\cdot\mathbf{r}|n,\mathbf{k}\rangle}{(E_{n,\mathbf{k}} - E_{n',\mathbf{k}} + \omega + i\eta)} + \frac{\langle n,\mathbf{k}|\mathbf{q}\cdot\boldsymbol{\mathcal{V}}|n',\mathbf{k}\rangle \langle n',\mathbf{k}|i\mathbf{q}\cdot\mathbf{r}|n,\mathbf{k}\rangle}{(E_{n,\mathbf{k}} - E_{n',\mathbf{k}})(E_{n,\mathbf{k}} - E_{n',\mathbf{k}} + \omega + i\eta)} \Bigg] + \mathcal{O}(q^3), \tag{C9}$$

whereas for $\mathbf{G}' \neq \mathbf{0}$, we obtain

$$\chi_0^{(1)S}(\mathbf{q},\mathbf{q}+\mathbf{G}';\omega) = \frac{2}{N_{\mathbf{k}} V_{\text{cell}}} \sum_{n,n'} \sum_{\mathbf{k}}^{\text{BZ}} f_{nn'} \Bigg[\frac{\langle n,\mathbf{k}|\mathcal{C}(z)|n',\mathbf{k}\rangle \langle n',\mathbf{k}|e^{i\mathbf{G}'\mathbf{r}'}|n,\mathbf{k}\rangle \langle n,\mathbf{k}|\mathbf{q}\cdot\mathbf{v}|n,\mathbf{k}\rangle}{(E_{n,\mathbf{k}} - E_{n',\mathbf{k}} + \omega + i\eta)^2} + \frac{\langle n,\mathbf{k}|\mathbf{q}\cdot\boldsymbol{\mathcal{V}}|n',\mathbf{k}\rangle \langle n',\mathbf{k}|e^{i\mathbf{G}'\mathbf{r}'}|n,\mathbf{k}\rangle}{(E_{n,\mathbf{k}} - E_{n',\mathbf{k}})(E_{n,\mathbf{k}} - E_{n',\mathbf{k}} + \omega + i\eta)} + \frac{\langle n,\mathbf{k}|\mathcal{C}(z)|n',\mathbf{k}\rangle \langle n',\mathbf{k}|e^{i\mathbf{G}'\mathbf{r}'}|n,\mathbf{k}\rangle}{(E_{n,\mathbf{k}} - E_{n',\mathbf{k}} + \omega + i\eta)} \Bigg] + \mathcal{O}(q^2). \tag{C10}$$

We first note that Eq. (C9) and Eq. (C10) contain, respectively, a term at first order in q and at zero order in q, which are not present in the corresponding bulk expressions. Nevertheless, from the comparison between the left-hand side and the right-hand side of Eq. (B4), we directly obtain that at lowest order in q, $\chi_0^{(1)S}(\mathbf{q},\mathbf{q};\omega)$ is proportional to q^2, and $\chi_0^{(1)S}(\mathbf{q},\mathbf{q}+\mathbf{G};\omega)$ is proportional to q. This proves that the terms at first order in q and at zero order in q, respectively, in Eq. (C9) and Eq. (C10) vanish.

Finally, one can easily show that the first terms in Eq. (C9) and in Eq. (C10) are equal to zero.

To summarize, we obtain, at the lowest order in q, that

$$\chi_0^{(1)S}(\mathbf{q},\mathbf{q};\omega) = \frac{2}{N_{\mathbf{k}} V_{\text{cell}}} \sum_{n,n'} \sum_{\mathbf{k}}^{\text{BZ}} f_{nn'} \frac{\langle n,\mathbf{k}|\mathbf{q}\cdot\boldsymbol{\mathcal{V}}|n',\mathbf{k}\rangle \langle n',\mathbf{k}|i\mathbf{q}\cdot\mathbf{r}|n,\mathbf{k}\rangle}{(E_{n,\mathbf{k}} - E_{n',\mathbf{k}})(E_{n,\mathbf{k}} - E_{n',\mathbf{k}+\mathbf{q}} + \omega + i\eta)}, \tag{C11}$$

$$\chi_0^{(1)S}(\mathbf{q},\mathbf{q}+\mathbf{G}';\omega) = \frac{2}{N_{\mathbf{k}} V_{\text{cell}}} \sum_{n,n'} \sum_{\mathbf{k}}^{\text{BZ}} f_{nn'} \frac{\langle n,\mathbf{k}|\mathbf{q}\cdot\boldsymbol{\mathcal{V}}|n',\mathbf{k}\rangle \langle n',\mathbf{k}|e^{i\mathbf{G}'\mathbf{r}'}|n,\mathbf{k}\rangle}{(E_{n,\mathbf{k}} - E_{m,\mathbf{k}})(E_{n,\mathbf{k}} - E_{n',\mathbf{k}} + \omega + i\eta)}. \tag{C12}$$

These expressions are similar to the usual expressions for matrix elements of $\chi_0^{(1)S}$; except the replacement $\langle n,\mathbf{k}|\mathbf{q}\cdot\mathbf{v}|n',\mathbf{k}\rangle \to \langle n,\mathbf{k}|\mathbf{q}\cdot\boldsymbol{\mathcal{V}}|n',\mathbf{k}\rangle$, which allows us to calculate the optical properties of a single surface.

At second order, the quantity $\chi_0^{(2)S}(\mathbf{q},\mathbf{q_1}+\mathbf{G_1},\mathbf{q_2}+\mathbf{G_2};\omega,\omega)$ is defined by

$$\chi_0^{(2)S}(\mathbf{q},\mathbf{q_1}+\mathbf{G_1},\mathbf{q_2}+\mathbf{G_2};\omega,\omega) = \frac{1}{L_z} \sum_{G_z} \tilde{\mathcal{C}}(-G_z)\chi^{(2)}_{0,\mathbf{G_z G_1 G_2}}(\mathbf{q},\mathbf{q_1},\mathbf{q_2};\omega,\omega), \tag{C13}$$

where $\chi_0^{(2)}$ is the Kohn-Sham second-order density response function [17].

Similarly to the first-order case, we obtained that the resulting expressions are similar to the expressions for bulk materials, where the only changes are due to the replacement of the matrix elements of $\mathbf{q}\cdot\mathbf{v}$ by matrix elements of $\mathbf{q}\cdot\boldsymbol{\mathcal{V}}$. The matrix elements associated to $\mathbf{q_1}$ and $\mathbf{q_2}$ are identical to those of the "usual" bulk formula. Note that an equivalent expression for the head of the matrix, $\chi^{(2)S}_{0,\mathbf{000}}$, can be found in Ref. [41].

APPENDIX D: RESPONSE FUNCTION TO THE TOTAL MACROSCOPIC CLASSICAL POTENTIAL AT SECOND ORDER

Let us define the total macroscopic classical potential [51] as

$$\hat{V}_{\text{mac}}[\rho] = \hat{V}_{\text{ext}} + v_{\mathbf{0}}\rho, \tag{D1}$$

where $v_{\mathbf{0}}$ is the long-range part of the Coulomb potential and $v_{\mathbf{0}}\rho$ stands for $\int d^3\mathbf{r_2} v_{\mathbf{0}}(\mathbf{r_1}-\mathbf{r_2})\rho(\mathbf{r_2})$. In the following, for the ease of notation, space and time integration will be implicitly assumed.

The density of the system reads as

$$\rho = \rho^{(0)} + \rho^{(1)}_{\text{ind}} + \rho^{(2)}_{\text{ind}}, \tag{D2}$$

where $\rho^{(0)}$ is the unperturbed density. Inserting this expression in Eq. (D1), yields

$$\hat{V}_{\text{mac}}[\rho] = \hat{V}^{(0)}_{\text{mac}} + \hat{V}^{(1)}_{\text{mac}} + \hat{V}^{(2)}_{\text{mac}}, \tag{D3}$$

where

$$\hat{V}^{(0)}_{\text{mac}} = v_{\mathbf{0}}\rho^{(0)}, \tag{D4}$$

$$\hat{V}^{(1)}_{\text{mac}} = \hat{V}^{(1)}_{\text{ext}} + v_{\mathbf{0}}\rho^{(1)}_{\text{ind}}, \tag{D5}$$

$$\hat{V}^{(2)}_{\text{mac}} = \hat{V}^{(2)}_{\text{ext}} + v_{\mathbf{0}}\rho^{(2)}_{\text{ind}}. \tag{D6}$$

We define the response functions $\bar{\chi}^{(1)}$ and $\bar{\chi}^{(2)}$ to that total macroscopic classical potential,

$$\rho^{(2)}_{\text{ind}} = \bar{\chi}^{(2)}\hat{V}^{(1)}_{\text{mac}}\hat{V}^{(1)}_{\text{mac}} + \bar{\chi}^{(1)}\hat{V}^{(2)}_{\text{mac}}. \tag{D7}$$

From this definition and the definition of the Kohn-Sham and the fully interacting response functions (see Ref. [17]), we obtain the two equations

$$\chi^{(2)} = \bar{\chi}^{(2)}[1 + v_{\mathbf{0}}\chi^{(1)}][1 + v_{\mathbf{0}}\chi^{(1)}] + \bar{\chi}^{(1)}v_{\mathbf{0}}\chi^{(2)}, \tag{D8}$$

$$\bar{\chi}^{(2)} = \chi_0^{(2)}[1 + \bar{v}\bar{\chi}^{(1)}][1 + \bar{v}\bar{\chi}^{(1)}] + \chi_0^{(1)}\bar{v}\bar{\chi}^{(2)}, \tag{D9}$$

where $\bar{v}$ is the Coulomb potential without its long-range part. For obtaining the second relation, we use

$$\hat{V}^{(1)}_{\text{tot}} = \hat{V}^{(1)}_{\text{mac}} + \bar{v}\rho^{(1)}_{\text{ind}}, \tag{D10}$$

$$\hat{V}^{(2)}_{\text{tot}} = \hat{V}^{(2)}_{\text{mac}} + \bar{v}\rho^{(2)}_{\text{ind}}. \tag{D11}$$

[1] M. C. Downer, B. S. Mendoza, and V. I. Gavrilenko, Surf. Interface Anal. **31**, 966 (2001).

[2] F. X. Wang, F. J. Rodríguez, W. M. Albers, R. Ahorinta, J. E. Sipe, and M. Kauranen, Phys. Rev. B **80**, 233402 (2009).

[3] B. Fluegel, A. Mascarenhas, J. F. Geisz, and J. M. Olson, Phys. Rev. B **57**, R6787 (1998).

[4] Y. R. Shen, Nature (London) **337**, 519 (1989).

[5] A. Savoia, D. Paparo, P. Perna, Z. Ristic, M. Salluzzo, F. Miletto Granozio, U. Scotti di Uccio, C. Richter, S. Thiel, J. Mannhart, and L. Marrucci, Phys. Rev. B **80**, 075110 (2009).

[6] J. I. Dadap, Z. Xu, X. F. Hu, M. C. Downer, N. M. Russell, J. G. Ekerdt, and O. A. Aktsipetrov, Phys. Rev. B **56**, 13367 (1997).

[7] P. Figliozzi, L. Sun, Y. Jiang, N. Matlis, B. Mattern, M. C. Downer, S. P. Withrow, C. W. White, W. L. Mochán, and B. S. Mendoza, Phys. Rev. Lett. **94**, 047401 (2005).

[8] Y. Jiang, P. T. Wilson, M. C. Downer, C. W. White, and S. P. Withrow, Appl. Phys. Lett. **78**, 766 (2001).

[9] M. H. Nayfeh, O. Akcakir, G. Belomoin, N. Barry, J. Therrien, and E. Gratton, Appl. Phys. Lett. **77**, 4086 (2000).

[10] B. D. Choudhury, P. K. Sahoo, R. Sanatinia, G. Andler, S. Anand, and M. Swillo, Opt. Lett. **40**, 2072 (2015).

[11] J. F. McGilp, M. Cavanagh, J. R. Power, and J. D. O'Mahony, Opt. Eng. **33**, 3895 (1994).

[12] C. Meyer, G. Lüpke, U. Emmerichs, F. Wolter, H. Kurz, C. H. Bjorkman, and G. Lucovsky, Phys. Rev. Lett. **74**, 3001 (1995).

[13] M. Cazzanelli, F. Bianco, E. Borga, G. Pucker, M. Ghulinyan, E. Degoli, E. Luppi, V. Véniard, S. Ossicini, D. Modotto, S. Wabnitz, R. Pierobon, and L. Pavesi, Nat. Mater. **11**, 148 (2012).

[14] T. V. Dolgova, A. I. Maidykovski, M. G. Martemyanov, A. A. Fedyanin, O. A. Aktsipetrov, G. Marowsky, V. A. Yakovlev, and G. Mattei, Appl. Phys. Lett. **81**, 2725 (2002).

[15] Y. Qiang An and S. T. Cundiff, Appl. Phys. Lett. **81**, 5174 (2002).

[16] G. Lüpke, Surf. Sci. Rep. **35**, 75 (1999).

[17] E. Luppi, H. Hübener, and V. Véniard, Phys. Rev. B **82**, 235201 (2010).

[18] R. Leitsmann, W. G. Schmidt, P. H. Hahn, and F. Bechstedt, Phys. Rev. B **71**, 195209 (2005).

[19] B. Adolph and F. Bechstedt, Phys. Rev. B **57**, 6519 (1998).

[20] E. Luppi, H. Hübener, and V. Véniard, J. Chem. Phys. **132**, 241104 (2010).

[21] M. L. Trolle, G. Seifert, and T. G. Pedersen, Phys. Rev. B **89**, 235410 (2014).

[22] C. Attaccalite and M. Grüning, Phys. Rev. B **88**, 235113 (2013).

[23] M. Grüning and C. Attaccalite, Phys. Rev. B **89**, 081102 (2014).

[24] N. Tancogne-Dejean, C. Giorgetti, and V. Véniard, Phys. Rev. B **92**, 245308 (2015).

[25] A. Selloni, P. Marsella, and R. Del Sole, Phys. Rev. B **33**, 8885 (1986).

[26] Y.-C. Chang and D. E. Aspnes, Phys. Rev. B **41**, 12002 (1990).

[27] F. Manghi, R. Del Sole, A. Selloni, and E. Molinari, Phys. Rev. B **41**, 9935 (1990).

[28] R. Del Sole and G. Onida, Phys. Rev. B **60**, 5523 (1999).

[29] M. Palummo, G. Onida, R. Del Sole, and B. S. Mendoza, Phys. Rev. B **60**, 2522 (1999).

[30] R. Del Sole and E. Fiorino, Phys. Rev. B **29**, 4631 (1984).

[31] R. Del Sole and A. Selloni, Phys. Rev. B **30**, 883 (1984).

[32] W. L. Mochán and R. G. Barrera, Phys. Rev. B **32**, 4984 (1985).

[33] W. L. Mochán and R. G. Barrera, Phys. Rev. B **32**, 4989 (1985).

[34] L. Reining, R. Del Sole, M. Cini, and J. G. Ping, Phys. Rev. B **50**, 8411 (1994).

[35] H. Sano, G. Mizutani, W. Wolf, and R. Podloucky, Phys. Rev. B **66**, 195338 (2002).

[36] B. S. Mendoza, A. Gaggiotti, and R. Del Sole, Phys. Rev. Lett. **81**, 3781 (1998).

[37] V. I. Gavrilenko, R. Q. Wu, M. C. Downer, J. G. Ekerdt, D. Lim, and P. Parkinson, Phys. Rev. B **63**, 165325 (2001).

[38] N. Arzate and B. S. Mendoza, Phys. Rev. B **63**, 125303 (2001).

[39] B. S. Mendoza, M. Palummo, G. Onida, and R. Del Sole, Phys. Rev. B **63**, 205406 (2001).

[40] J. E. Mejía, B. S. Mendoza, M. Palummo, G. Onida, R. Del Sole, S. Bergfeld, and W. Daum, Phys. Rev. B **66**, 195329 (2002).

[41] S. M. Anderson, N. Tancogne-Dejean, B. S. Mendoza, and V. Véniard, Phys. Rev. B **91**, 075302 (2015).

[42] B. S. Mendoza and W. L. Mochán, Phys. Rev. B **53**, R10473(R) (1996).

[43] J. Mejía and B. Mendoza, Phys. Status Solidi A **188**, 1393 (2001).

[44] H. Ehrenreich, in *The Optical Properties of Solids*, Proceedings of the International School of Physics "Enrico Fermi", edited by J. Tauc (Academic, New York, 1966), p. 106.

[45] C. Hogan, R. Del Sole, and G. Onida, Phys. Rev. B **68**, 035405 (2003).

[46] B. S. Mendoza, F. Nastos, N. Arzate, and J. E. Sipe, Phys. Rev. B **74**, 075318 (2006).

[47] A. Incze, R. Del Sole, and G. Onida, Phys. Rev. B **71**, 035350 (2005).

[48] S. Botti, A. Schindlmayr, R. Del Sole, and L. Reining, Rep. Prog. Phys. **70**, 357 (2007).

[49] Note that when exchange and correlation effects can be described by a scalar kernel, it can be added as a postprocessing.

[50] N. Tancogne-Dejean, C. Giorgetti, and V. Veniard (unpublished).

[51] G. Onida, L. Reining, and A. Rubio, Rev. Mod. Phys. **74**, 601 (2002).

[52] X. Gonze, J.-M. Beuken, R. Caracas, F. Detraux, M. Fuchs, G.-M. Rignanese, L. Sindic, M. Verstraete, G. Zerah, F. Jollet *et al.*, Comput. Mater. Sci. **25**, 478 (2002).

[53] N. Troullier and J. L. Martins, Phys. Rev. B **43**, 1993 (1991).

[54] http://www.dp-code.org/ (unpublished).

[55] H. Hübener, E. Luppi, and V. Véniard (unpublished).

[56] Y. Q. An and S. T. Cundiff, Phys. Rev. B **67**, 193302 (2003).

[57] M. Falasconi, L. Andreani, A. Malvezzi, M. Patrini, V. Mulloni, and L. Pavesi, Surf. Sci. **481**, 105 (2001).

[58] Y. Q. An, R. Carriles, and M. C. Downer, Phys. Rev. B **75**, 241307 (2007).

[59] W. Daum, H.-J. Krause, U. Reichel, and H. Ibach, Phys. Rev. Lett. **71**, 1234 (1993).

[60] U. Höfer, Appl. Phys. A **63**, 533 (1996).

[61] M. B. Yilmaz, A. Rajagopal, and F. M. Zimmermann, Phys. Rev. B **69**, 125413 (2004).

[62] R. Del Sole and R. Girlanda, Phys. Rev. B **48**, 11789 (1993).

[63] M. Palummo, N. Witkowski, O. Pluchery, R. Del Sole, and Y. Borensztein, Phys. Rev. B **79**, 035327 (2009).

[64] P. Parkinson, D. Lim, R. Büngener, J. Ekerdt, and M. Downer, Appl. Phys. B **68**, 641 (1999).

[65] S. M. Anderson, N. Tancogne-Dejean, B. S. Mendoza, and V. Véniard, Phys. Rev. B **93**, 235304 (2016).

[66] The difference between Fig. 4 and Fig. 10 is due to the use of the scissor in the latter.

[67] J. J. H. Gielis, P. J. van den Oever, B. Hoex, M. C. M. van de Sanden, and W. M. M. Kessels, Phys. Rev. B **77**, 205329 (2008).

[68] S. Botti, F. Sottile, N. Vast, V. Olevano, L. Reining, H.-C. Weissker, A. Rubio, G. Onida, R. Del Sole, and R. W. Godby, Phys. Rev. B **69**, 155112 (2004).

[69] C. Kittel and C.-y. Fong, *Quantum Theory of Solids*, Vol. 33 (Wiley, New York, 1963).

[70] C. Aversa and J. E. Sipe, Phys. Rev. B **52**, 14636 (1995).